AD-A155 776 (NAT)FE(NN'X) SPECTRA AT 655 MEV(U) ARMY MILITARY PERSONNEL CENTER ALEXANDRIA VA M A HAMILTON 05 JUN 85 1/1

UNCLASSIFIED F/G 20/8 NL

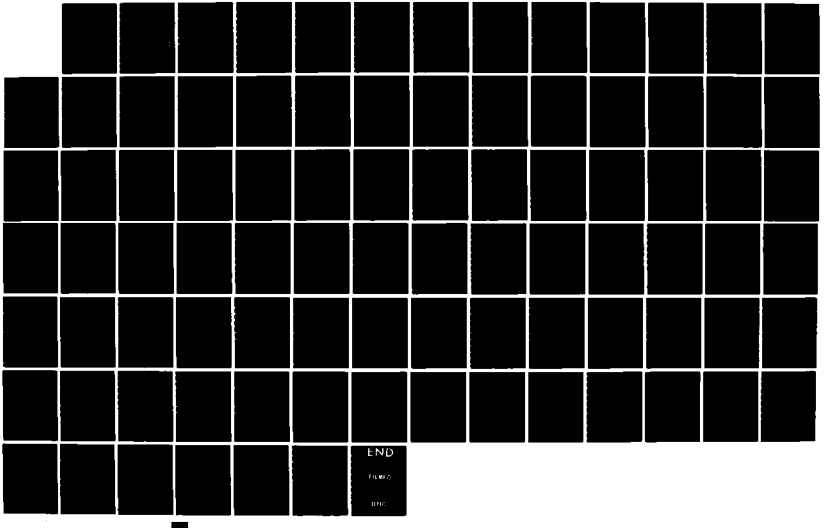

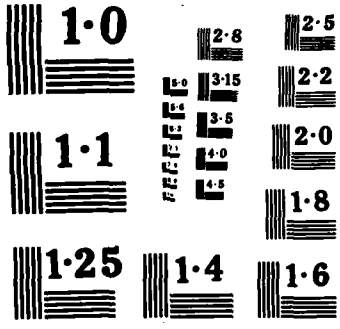

(2)

$^{nat}Fe(n,n'x)$ Spectra at 65.5 MeV

CPT Michael A. Hamilton
HQDA, MILPERCEN (DAPC-OPA-E)
200 Stovall Street
Alexandria, VA 22332

Final Report, 5 June 1985

Approved for public release; distribution is unlimited.

A thesis submitted to the University of California, Davis, CA
in partial fulfillment of the requirements for the degree of Master of Arts.

SECURITY CLASSIFICATION OF THIS PAGE *(When Data Entered)*

REPORT DOCUMENTATION PAGE		READ INSTRUCTIONS BEFORE COMPLETING FORM
1. REPORT NUMBER	2. GOVT ACCESSION NO. A155776	3. RECIPIENT'S CATALOG NUMBER
4. TITLE *(and Subtitle)* ^{nat}Fe(n,n'x) Spectra at 65.5 MeV		5. TYPE OF REPORT & PERIOD COVERED Final Report, 5 June 1985 6. PERFORMING ORG. REPORT NUMBER
7. AUTHOR(s) CPT Michael A. Hamilton		8. CONTRACT OR GRANT NUMBER(s)
9. PERFORMING ORGANIZATION NAME AND ADDRESS Student HQDA, MILPERCEN, (DAPC-OPA-E) 200 Stovall Street Alexandria, VA 22332		10. PROGRAM ELEMENT, PROJECT, TASK AREA & WORK UNIT NUMBERS
11. CONTROLLING OFFICE NAME AND ADDRESS HQDA, MILPERCEN ATTN: DAPC-OPA-E 200 Stovall Street Alexandria, VA 22332		12. REPORT DATE 5 June 1985 13. NUMBER OF PAGES 78
14. MONITORING AGENCY NAME & ADDRESS *(if different from Controlling Office)*		15. SECURITY CLASS. *(of this report)* Unclassified 15a. DECLASSIFICATION/DOWNGRADING SCHEDULE

16. DISTRIBUTION STATEMENT *(of this Report)*

Approved for public release; distribution unlimited.

17. DISTRIBUTION STATEMENT *(of the abstract entered in Block 20, if different from Report)*

Same

18. SUPPLEMENTARY NOTES

Thesis. Submitted in partial satisfaction of the requirements for the degree of MASTER OF ARTS in Physics in the Graduate Division of the University of California, Davis.

19. KEY WORDS *(Continue on reverse side if necessary and identify by block number)*

1. Giant Resonance
2. (n,n'x)
3. Neutron matrix elements
4. Proton matrix elements
5. Multiwire Chamber Detector
6. Intermediate energy neutrons
7. (n,n'x) spectra

20. ABSTRACT *(Continue on reverse side if necessary and identify by block number)*

The first spectra from the U.C. Davis (n,n'x) detection facility are presented for 65.5 MeV incident neutrons on a ^{nat}Fe target. The experimental system is explained along with analysis methodology. Elastic and continuum spectra are presented from 14 to 24 degrees with cross section tabulation. Cross section comparisons are made between 20 degree (n,n'x) and 20 degree (p,p'x) data at 61 MeV and the ratio of neutron to proton matrix elements has been obtained. The first evidence

DD FORM 1 JAN 73 1473 EDITION OF 1 NOV 65 IS OBSOLETE

SECURITY CLASSIFICATION OF THIS PAGE *(When Data Entered)*

20. (cont.)
of a (n,n'x) giant resonance has been detected. [illegible] include:

$^{nat}Fe(n,n'x)$ Spectra at 65.5 MeV

By

CPT MICHAEL A. HAMILTON
B.S. (United States Military Academy, West Point) 1976

THESIS

Submitted in partial satisfaction of the requirements for the degree of

MASTER OF ARTS

in

Physics

in the

GRADUATE DIVISION

of the

UNIVERSITY OF CALIFORNIA

DAVIS

Approved: .....

.....

.....

Committee in Charge

Deposited in the University Library .....
Date Librarian

Table of Contents

LIST OF FIGURES

LIST OF TABLES

ABSTRACT

The first spectra from the U.C. Davis (n,n'x) detection facility are presented for 65.5 MeV incident neutrons on a ^{nat}Fe target. The experimental system is explained along with analysis methodology. Elastic and continuum spectra are presented from 14 to 24 degrees with cross section tabulation. Cross section comparisons are made between 20 degree (n,n'x) and 20 degree (p,p'x) data at 61 MeV and the ratio of neutron to proton matrix elements has been obtained. The first evidence of a (n,n'x) giant resonance has been detected.

ACKNOWLEDGEMENTS

With any experiment there are several individuals to be thanked for their time and effort in making an idea a reality. I am especially grateful to Professor F. Paul Brady, first for understanding the time limitations placed on me by the Army, second for allowing me to conduct this experiment, and third, for his guidance, perception and professionalism throughout the experimental and analysis period. Special thanks also go to Dr. Timothy Ford who was directly responsible for introducing me to the science of neutron detection and neutron data analysis. Without his expertise in the experimental system and creativity in the software development, this experiment could not have been completed in such a short time. Thanks also go to the entire neutron group including Juan Romero, Carlos Castaneda, Jim Drummond and Bruce McEachern for their willingness to help whenever it was needed. I also want to acknowledge Dr. John Jungerman and Dr. Thomas Cahill for their help in preparing this manuscript and Madelin Cameron for so efficiently typing it. Lastly, I want to thank my wife Becky, whose help, understanding and advice made this project such a rewarding experience.

PART I

INTRODUCTION

With the technology available in this century, we have successfully identified the macro-structure of the nucleus and determined many of its properties by means of a series of nucleon collision experiments. However, our experimental techniques and collision energies have proven to be inadequate to accurately measure direct (n,n'x) continuum spectra. In the future, such information would be of assistance in better understanding the interrelationship between the protons and neutrons of the nucleus. When combined with other results, such as (p,p'x) measurements, the data may allow a better insight into the infrastructure of the nucleons and the constituent quarks and other sub-nucleons with which they interact.

The observation of the continuum and Giant Resonances (GR) [especially Giant Quadrupole Resonance (GQR)] have been of particular interest in the last few years, and have been measured through the excitation of nuclei by intermediate energy incident particles such as protons. Up to this time however, incident neutron experiments have not been conducted even though (n,n'x) reaction results are considered to be complementary to the proton data. With such complementary data available, theorists would have a better chance of understanding the GR phenomena. This shortcoming can be attributed to two main problems in examining (n,n'x) reactions. First, a nearly true, high intensity monoenergetic neutron beam has been lacking, and second, a procedure other than Time of Flight method (TOF) has been needed to measure neutron energies. (TOF, besides needing huge laboratory areas, proved

inadequate to properly separate elastic and inelastic scattering of lower energy neutrons in the "tail" from those in the continuum of the reactions due to the main energy peak.)

The two problems have been all but resolved by advances in technique made by the Neutron Group at the University of California (Davis). The availability of the 76 inch isochronous cyclotron and neutron facility at Crocker Nuclear Laboratory (CNL), and the development of Multi-Wire-Chamber (MWC) detectors created a unique opportunity to investigate, for the first time, (n,n'x) continua over a wide range of intermediate energies. This opportunity has made possible an effort to develop, and test, a facility that will measure the (n,n'x) continuum and identify giant resonances within that continuum for selected angles, energies and targets. With such data, initial rudimentary comparisons can be made between the (p,p'x) and (n,n'x) continua.

PART II

THEORY

This section is intended to provide a brief theoretical framework required to understand the notion of GR's and to assist in understanding the interpretation of the experimental results. To meet these goals, the intermediate energy nucleon spectrum is explained, along with the shell model and hydrodynamic view of the nucleus. These ideas are intended to assist the reader in conceptualizing GR transitions. Also, some quantum mechanics are introduced, not only to better describe the interactions in the nucleus but, also to give us a few brief checks as to the validity of our conclusions.

When discussing (n,n'x) spectra, since up till now no (n,n'x) data had been available, (p,p'x) results have been often used to illustrate the shape of the expected spectrum for (n,n'x). In figure 1 a representation of a (p,p'x) energy spectrum is presented for an incident proton beam energy of 65 MeV.

At the high energy end the proton and expected neutron data is characterized by the elastic peak and discrete low lying states of excitation on the order of a few MeV. The interaction (normally one-step) corresponding to these excitations is a fast, or direct reaction, taking on the order of 10^{-22} sec. This interaction allows no time for the energy to be shared among the incident and more than one or two of the target nucleons.

At the opposite end of the spectrum, the evaporation peak results from the incident particle sharing its energy with all or a large fraction of the target nucleons, forming a compound system. These

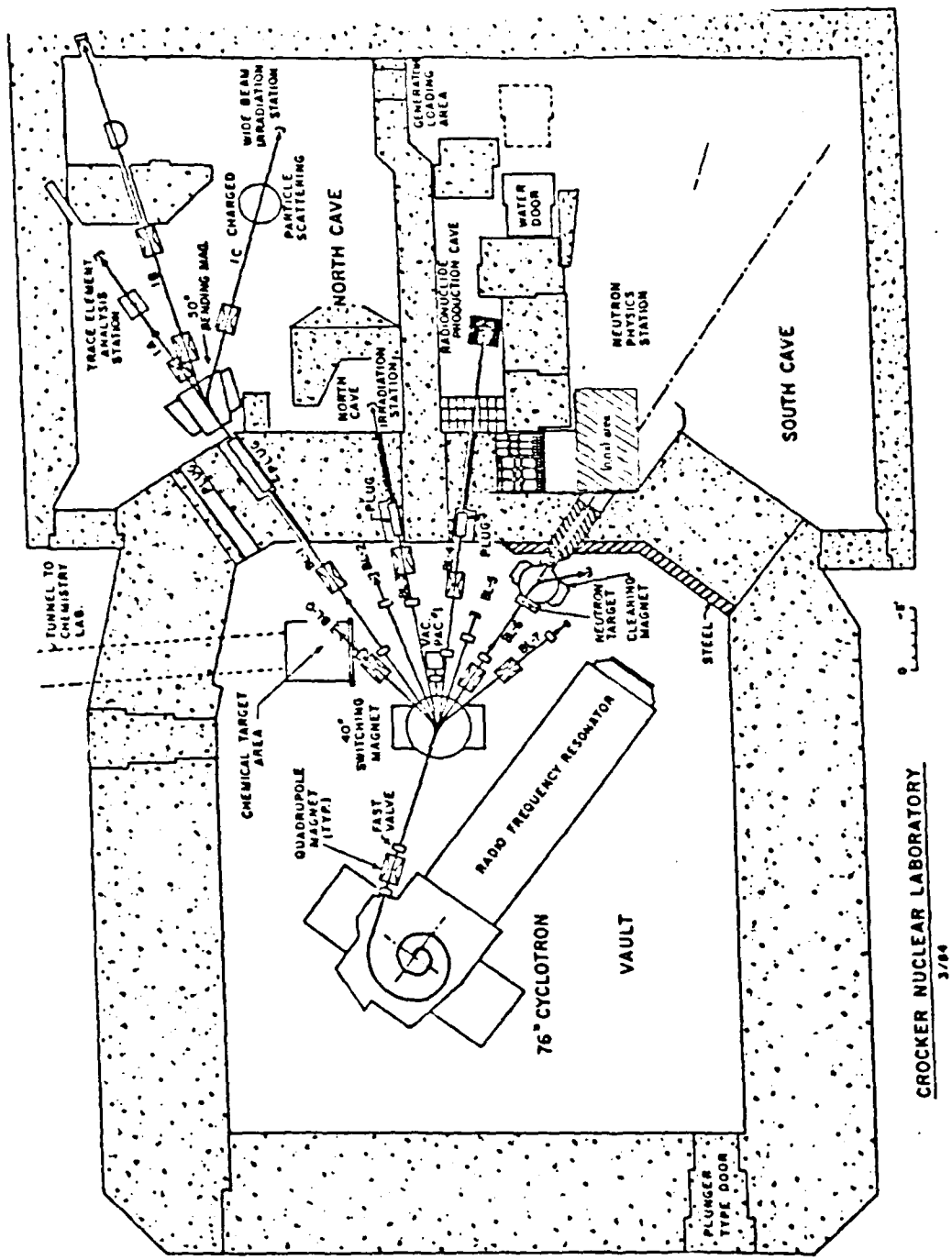

Figure 3

Experimental areas at Crocker Nuclear Lab.

PART III

THE EXPERIMENTAL EQUIPMENT AND SET-UP

In discussing the laboratory set-up, it is important to first describe the two unique elements of equipment available at CNL: the monoenergetic neutron beam and the Multi-Wire Chambers. The rest of the system will be described with special importance being placed on those elements singular to a (n,n'x) experiment.

The 76 inch isochronous cyclotron at UC Davis (see figure 3) is one of the few facilities in the country able to produce a nearly monoenergetic high energy neutron beam (polarized and unpolarized). Protons are accelerated by the cyclotron and formed into bursts of approximately 1 ns in duration. They are then focused by a quadrupole magnet and directed to the production target by means of a 40" switching magnet. Before striking the target, the beam passes by a Beam Pickoff Probe (BPO). The BPO detects the beam burst and sends a signal which is used as a TOF reference. The protons continue to the lithium production target where the neutron beam is produced by means of a $^{7}Li(p,n)^{7}Be$ reaction. (This reaction is due to transitions to the ground and first state in ^{7}Be.) The beam can be adjusted from a few MeV up to 70 MeV with a current of 10 to 20uA depending on the thickness of the lithium target used. The resulting neutron beam is almost monoenergetic with a peak that typically ranges from .5 to 1.0 MeV FWHM (full width, half maximum). Even under the best conditions, as found here at Crocker Nuclear Laboratory, the production beam is only nearly monoenergetic (the spectrum peak contains 60% of the neutrons) and therefore a small,

comparisons are made. Also the use of a natural iron target (92% ^{56}Fe) may cause some minor disparity in the values. However, even with these differences the (p,p'x) continuum results should generally hold for direct comparison.

With this brief overview of the theory of GR's and the continuum we now proceed to explain the experimental set-up used for (n,n'x) detection.

It is expected that the continuum and GR of (p,p'x) and (n,n'x) should be similar in nature, i.e. in shape and approximate cross section, for particular energies and angles.[9] Since the ^{56}Fe nucleus is not single closed shell (SCS) valence for neutron or protons, the neutron multipole matrix element, (M_n) and the proton matrix element (M_p) are thought to be related by

$$M_n/M_p = N/Z \qquad [14]$$

(For ^{56}Fe N/Z = 1.15).

The nucleon-nucleon potential for a given particle x interacting with another particle y is represented by V_{xy}. It is commonly expected the potential for proton-neutron scattering (V_{pn}) is equal to that for neutron-proton scattering (V_{np}) but approximately 3 times greater than the potential for a neutron-neutron (V_{nn}) or proton-proton (V_{pp}) interaction (*i.e.* $V_{pn}=V_{np}=3V_{nn}=3V_{pp}$).[10] It can then be concluded that protons interact predominately with neutrons and neutrons with protons in the nucleus. Therefore one expects (to first order) that the ratio of the relative cross sections for a (n,n'x) and (p,p'x) reaction could be represented by[11]

$$\sigma(n,n'x)/\sigma(p,p'x) = V_{np}M_p + V_{pp}M_n/V_{pn}M_n + V_{pp}M_p = .93 \text{ (for eq. [14])}. \qquad [15]$$

Therefore the magnitude of the cross sections for (n,n'x) results is expected to be .93 the value of that for a (p,p'x) reaction and a neutron-proton comparison should be a good initial check and starting point in validating the (n,n'x) results presented here. Due to the different properties of protons and neutrons, it is expected that there will be minor variations in cross section and spectra shape when

With the β terms having been determined the EWSR% can then be calculated using the equation

$$EWSR\% = (CG)\beta_L^2(expt)/\beta_L^2(100\%) \qquad [13]$$

where CG = Clebsch-Gordon coefficient (for an E2 transition it is equal to 1).

Once calculated, a collective transition is considered to have taken place if the exhausted strength value, EWSR%, is greater than or equal to 10%.

Putting all this information together, we can better understand what is occuring in the nucleus and the resultant energy spectra expected for this experiment. The incident neutron approaches the target nucleus and interacts with one of its nucleons transferring some of its momentum to the rest of the system. Due to this transfer there is a probability of nucleons collectively jumping from one major shell and subshell to other major shells and subshells as described above. Usually the original incident neutron, or via exchange some other nucleon, leaves the system with some loss of kinetic energy compared to that of the incident neutron. This difference in energy of the "prime" projectile nucleon (for our experiment a neutron) can reflect the quanta of energy needed to make the collective excitation. The observation of a hump in one section of the energy spectrum below the elastic peak can constitute a GR once the transition is verified as being collective by use of the EWSR. Because of the nature of the excitation in GR we see a small spreading of this transfer energy due to the quantum mechanical sharing or mixing of shell states. If looked at more simplistically it is due to the quanta of energy being added to nucleons that start in different subshells and thus a broadening of the excitation peak.

For a ground state nucleus, this $2\hbar\omega$ transition would result in an excitation (E) restricted to a small section of the energy spectrum. So the EWSR would reduce to

$$C = S_L/S^{SP}\ E = 4.83(A^{1/3})L(L+3)MeV/mE = 241(A^{1/3})MeV/mE \qquad [8]$$

where $R = 1.2(A^{-1/3})fm$, and

$h^2 = 41.8\ MeV(fm^2)$.

In this experiment, with an incident neutron of mass approximately one and A = 56 (minor isotopes of natural iron will not really affect our result), then

$$C = 185/E, \qquad [9]$$

where the result C must be greater than or equal to 10 to verify that a collective transition is possible.

It is clear that so far the EWSR has only given us a very crude rule to go by. When investigating hadron scattering, a more precise method must be used to check what fraction of the EWSR strength has actually been exhausted. To do this, first an experimental deformation parameter $[\beta_L^2(expt)]$ must be obtained. This is accomplished by comparing the experimental value for the cross section of the area of interest, $\sigma(expt)$, with that predicted for the giant resonance by the program "DWUCK" using the distorted wave Born approximation (DWBA) where

$$\beta_L^2(expt) = \sigma(expt)/\sigma(DWUCK). \qquad [10]$$

For 100% of the strength to be exhausted with the case T=S=0, in terms of EWSR can be represented as

$$\beta_L^2(100\%) = 2\pi(h^2)L(2L+1)/3mA(R^2)E=60.8L(2L+1)MeV/A^{5/3}E. \qquad [11]$$

Using natural iron where A=56 and a $2\hbar\omega$ transition taking place

$$\beta_L^2 = .74\ MeV/E \qquad [12]$$

strength to a single particle estimate for the same transition. The most often used sum rule today is the Energy Weighted Sum Rule (EWSR) limit since estimates on its value can be made that are nearly model independent. The EWSR can be defined as

$$S_{EW}^{TL} = (E_f - E_i)\langle n|Q_{TLO}|0\rangle^2 \qquad [6]$$

where E_i and E_f represent the transitions initial and final states. It is possible that collective transition has taken place when the EWSR divided by the single particle estimate (S^{SP}) is greater than or equal to approximately 10.

Estimates on the EWSR value can be more easily made by assuming a uniform mass distribution for the nucleus, a nucleon-nucleon interaction that is basically velocity independent and T=S=0 then[7]

$$S_{EW}^{OL} = (h^2)AL(2L+1)\langle r(2L-2)\rangle/8\pi M$$

$$= 3A(h^2)L(2L+1)R(2L-2)/8\pi M \qquad [7]$$

where M = the nucleon mass,

A = the nuclear mass, and

$R = 1.2(A^{-1/3})$fm.

Using this form of the equation for the sum rule, the most simple case to calculate and check for collective motion is that for an E2 transition. Such a transition is prevalent in (p,p'x) data and is expected to occur for the (n,n'x). For E2, $0\hbar\omega$ and $2\hbar\omega$ transitions are the only ones possible and expect that these two collective transitions should exhaust the sum rule. But by the above equation it is clear that the $0\hbar\omega$ case does not contribute significantly to the transitions sum; therefore, most of the E2 collective strength must come from the $2\hbar\omega$ transition.

major shells (i.e. if L=1 the nucleon makes a transition from N to N+1). It should be noted that the sum over (i) above includes all nucleons of the nucleus but only those having the correct quantum numbers will coherently contribute to the resonant transition.

It is well known that the ground state (gs) of a nucleus contains a set of orbitals all, or most, of the same phase. This set of orbitals can be represented as a linear combination of states such as

$$gs = ag + bg + cg + dg + \ldots \qquad [2]$$

The multipole operator acting on these states connects them to a respective set of GR states (rs). This second set of states can also be expressed as a superposition or coherent mixture and represented as

$$rs = ar + br + cr + dr + \ldots \qquad [3]$$

We can therefore represent the single particle matrix element for a nucleon transition between the ground state (L=0) and some other resonant state as

$$S^{sp} = \langle rs|Q_{OLM}|gs\rangle = \frac{1}{(4\pi)^{\frac{1}{2}}} \int [(u_L(r)r^L u_o(r)]r^2dr. \qquad [4]$$

Here the u terms represent their respective wave functions. This integral can be estimated by the Lth moment of the density distribution $\rho(r)$ of the target nucleus (assuming a uniform mass distribution for the nucleus)[6]:

$$\langle r^L\rangle = \int r^L\rho(r)dr/\int\rho(r)dr = \int r^L 4\pi r^2dr/1.25R^3 = (3/L+3)R. \qquad [5]$$

When looking for collective motion in the nucleus, the regular appearance of a broad peak in the energy spectrum is the first circumstantial evidence of a giant resonance. This, however, must be verified by the use of what are usually called "sum rules". The sum rule verification involves the comparison of the measured transition

particle experiments it has yet to be observed by (n,n'x) interaction, which, is one of the purposes of this experiment.

It follows that octopole resonances (E3) excitations are of $1\hbar\omega$ and $3\hbar\omega$, and that E4 are of $0\hbar\omega$, $2\hbar\omega$, and $4\hbar\omega$. Higher order resonances are thought to exist but their presence has not been positively verified experimentally.[4]

Although the above descriptions assist us in gaining a physical feeling for what is occuring, a correct description of the GR excitation must relate more directly to the quantum mechanical view of matter.

Nuclear collective modes are classified by their multipole order V, where V=V(T,L,S). Where (T,L,S) are the quantum numbers transferred to the nucleus. T represents the isotopic spin (T=0 is isoscalar, T=1 is isovector). L is the angular momentum quantum number of the modes and S represents the spin mode (S=0, then spin-up and spin-down modes oscillate in phase, S=1 when they oscillate out of phase).

In defining multipole modes the GR transition operator is,

$$Q_{TLM} = \sum_{i}^{A} r_i^L Y_{LM}(i) \qquad \text{for T=0 (often called the mass multipole operator),}$$

or [1]

$$Q_{TLM} = \sum_{i}^{A} \tau_{3i} r_2^L Y_{LM}(i) \qquad \text{for T=1;}$$

here Y_{LM} = eigenfunction of orbital angular momentum,

r_j = rms charge radius of the ground state, and

τ_{3i} = isospin operator.[5]

The multipole operator can excite a nucleon by, at most, $1\hbar\omega$ from the ground state. Therefore the nucleon can be excited up, at most, L

shell energy difference is less and is believed to be caused by the attractive interaction. This repulsive and attractive interaction helps to explain the deviations from the $41/A^{1/3}$ factor described above.[3]

The hydrodynamic and shell model of the nucleus makes it easier to imagine the convolutions the nucleus is undergoing. Using these ideas different types of GR are described and explained below.

Monopole resonance (E0), or breathing mode, is a symmetric expansion and contraction of the nuclear sphere. It is theorized to exist and has been observed in several nuclei due to collision excitation by several different scattering particles including electrons and protons.

Giant dipole resonance (GDR)(E1) is isovector in nature and can be described as collective transitions spanning $1\hbar\omega$($\Delta N=1$, see figure 2). GDR, the first GR to be observed, is believed to be due to the oscillation of the neutrons against protons causing a separation between the center of mass and charge in the nucleus. This resonance is generally the most prominent resonance observed in the laboratory and can be excited by most particles of sufficient energy including electrons, protons, alpha particles and photons (by which it was discovered).

For giant quadrupole resonance (GQR)(E2) there are two different sets of collective transitions possible as seen in the figure. The $\Delta N=0$ ($0\hbar\omega$s) transition is made up of transitions between subshells of a major shell, and the $\Delta N=2$ transition between shells N and N+2 would have energy of $2\hbar\omega$. GQR is a 3D expansion of the nuclear sphere which causes the nucleus to oscillate between different oblate or prolate shapes. Although this resonance has been observed in (p,p'x), electron and alpha

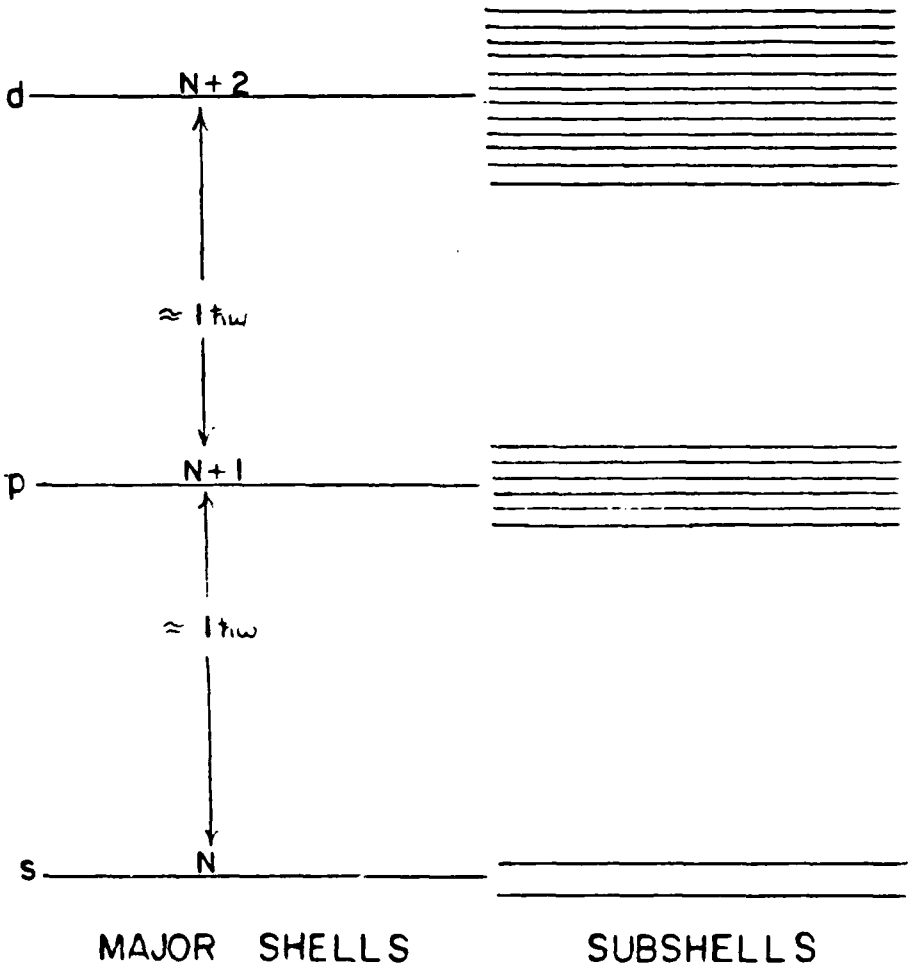

Figure 2

Single particle transitions between shell model states of a representative nucleus.

transition is caused by incident particle interacting and the sharing energy with the individual particles within the nucleus.

Single particle transitions between shell model states of a representative nucleus are shown in figure 2. The major shells are denoted by N=i (i=1,2,...), with associated subshells also being shown. In the shell model the major shells are thought to be separated by approximately $41/A^{1/3}$ MeV (10.7 MeV for ^{56}Fe).[2] To explain GR by this model alone we are to believe that many nucleons make these transitions (at one time) to create the coherent motion observed.

Although the simple shell model gives us an idea about what might be happening at nucleon level, it does not fully describe the ordered group transitions observed. Depending on the nuclei, the GR's have been experimentally located at higher or lower energies than predicted by the $41/A^{1/3}$ MeV factor of the simple shell model. This phenomena must be explained using a more complicated model of the nucleus with more complicated nucleon-nucleon interactions.

A first step in this effort is carried out by using a hydrodynamic model of interaction. This macroscopic description involves the superposition of many particle excitations, both singular and multiple. The number of excitations possible is limited due to the Pauli exclusion principle which forbides two ½ħ particles from being in the same state of the system. Associated with this model, is a representation of the nuclear system as acting like the oscillations of a "liquid drop". If the interaction is isovector in nature (neutrons and protons moving out of phase) the difference in the shell energy mentioned above is believed to be caused by the repulsive nature of the nucleon interaction. In the isoscalar case (neutrons and protons collectively moving in phase) the

overlapping compound states tend to survive for long time periods compared to the orbital period of a nucleon (10^{-22} sec), or the time for a fast (elastic) reaction. Later in time, by chance, the energy is localized to allow the decay by the emission of one nucleon or a small group.

The intermediate energy region, the one being examined in this paper for (n,n'x) interaction, is characterized by structures which are broad in excitation energy on the order of 10 MeV. The broad peaks, called giant resonances (GR), are observed in many nuclei and represent a general behavior of nuclear dynamics. It is a highly collective mode of nuclear excitation in which a large fraction of the nucleons are considered to participate. The intermediate energy region also embraces contributions attributed to multistep or preequilibrium processes. This includes other more complicated configurations including many particle compound states.[1]

To more closely examine the nature of GR, it is traditional to consider the interaction from two different viewpoints. The first, the microscopic point of view, is based on the shell model and nucleon-nucleon interactions. The second model, or hydrodynamic view, is macroscopic in nature and considers the interaction in terms of the entire nucleus. Each model helps to explain certain properties we observe in the nucleus, and so, the combination of the two allows us to at least partially discern what produces the GR.

From the shell model perspective, giant resonances can be considered to result from the quantum mechanical transitions of neutrons or protons within the nucleus from one major shell single particle orbit, to a single particle orbit of another major shell. The

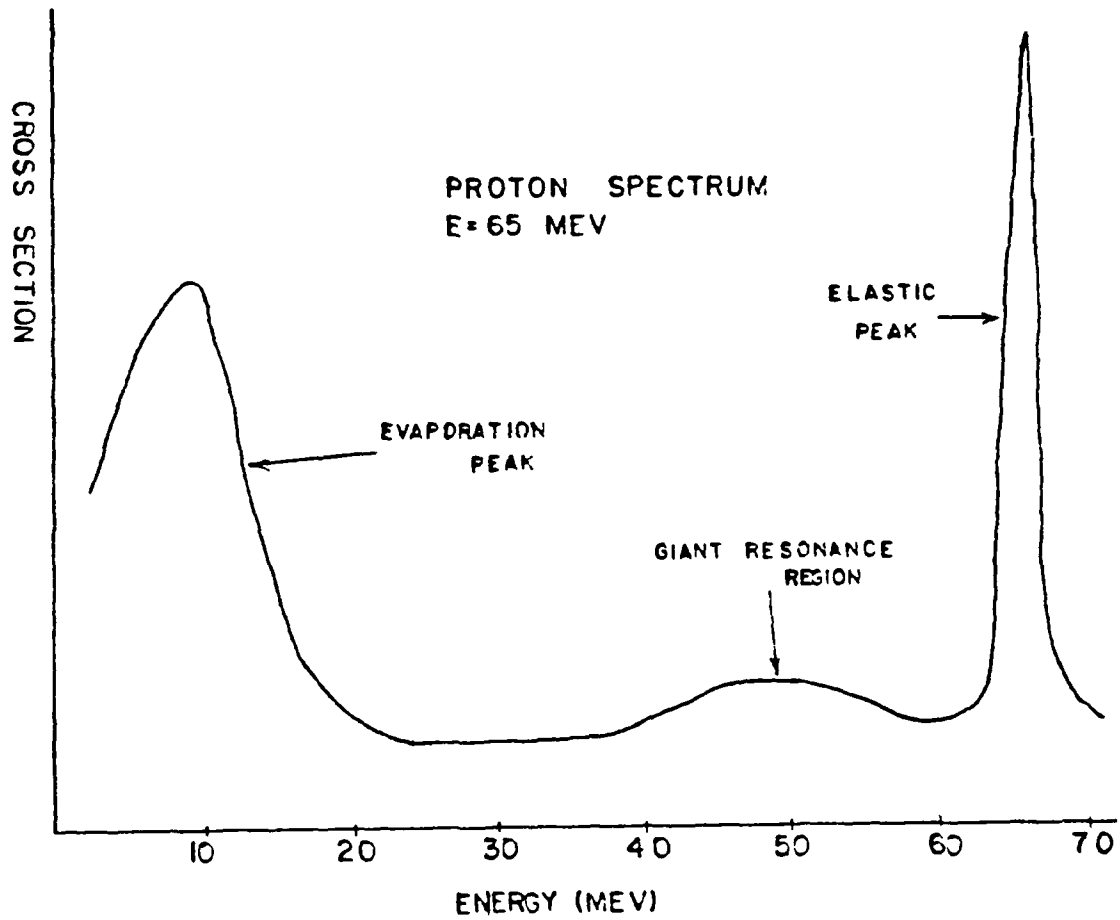

Figure 1

Representative (p,p'x) energy spectrum for incident protons at 65 MeV.

flat, low energy "tail" exists behind the main neutron energy peak in the beam.

As mentioned in the introduction, TOF is not a very useful method for measuring (n,n'x) or (p,p'x) spectra. For this reason, the Multi-Wire Chambers (MWC) were introduced to meet the needs for a system that required small detector distances and therefore a small laboratory size, yet permitted the measurement of neutron and proton scattering over a wide range of energies and scattering angles.

Dr. Chris Morris (Los Alamos National Laboratory) developed a wire chamber detector that proved adequate for these experimental requirements. Using Morris's design, similar wire chambers were developed by Dr. F.P. Brady and the Neutron Group at CNL, with the first tests taking place in 1981. The small detector distances needed for MWC's means large solid angle, and therefore, measurements of proton or neutron scattering in a wide range of scattering angles at one time. Also, the small laboratory size reduces the background interference; secondary scattering of neutrons or protons from the walls, floor and ceiling have little probability of re-entering the system. By making minor modifications of MWC (p,p'x) set-up the neutron group was able to create the first prototype of the (n,n'x) detection system using software modified by Dr. T. Ford of the Neutron Group. The same year, Dr. Ford also made the initial (n,n'x) runs proving the accuracy of the new neutron detection system.[12]

It should be noted that major parts of the detector system to be discussed have been tested extensively to investigate reactions such as (n,d) and (n,p) by the Neutron Group at CNL. A prototype setup similar to the one used in this experiment was tested during preliminary (n,n'x)

runs in 1981.[13] With the above facts in mind, we now begin a trek through the set-up in the sequence experienced by a nucleon during the experiment.

Upon exiting the production target, the neutron beam is made up of a mixture of non-reactant protons and recoil neutrons. This mixed beam passes through a clearing magnet which deflects the protons into a Faraday Cup where a current integrator gives an indication of neutron beam flux strength (see figure 4). (During the experiment a current of 12uA was maintained.) Any H^{o} particles in the beam lose their electron upon passing through the stripping foil (shown in figure 4) and the resultant proton is deflected by the magnet into wall near the Faraday Cup. The now pure neutron beam passes through a collimator and into the experimental area. Upon exiting the collimator the beam size is 3.8 cm high, 1.8 cm wide and typically carries a flux of 10^{6} neutrons per second. After passing through 30 cm of air the beam strikes the target suspended in the target ladder.

The Target

After careful study, the best compromise between theoretical and practical applications, resulted in a choice of iron (Fe) for the target. Indications were good that a resultant giant resonance could be observed due to incident 65.5 MeV neutrons.[14]

The natural iron target was .969 cm thick, 1.79 cm high and 4 cm long. As mounted, only 1.8 by 1.79 cm target area was presented to the beam in an effort to decrease the angular resolution error that would be caused by a target of larger size. The chosen thickness of the Fe was designed to produce the maxim number of neutron-atom collisions, yet

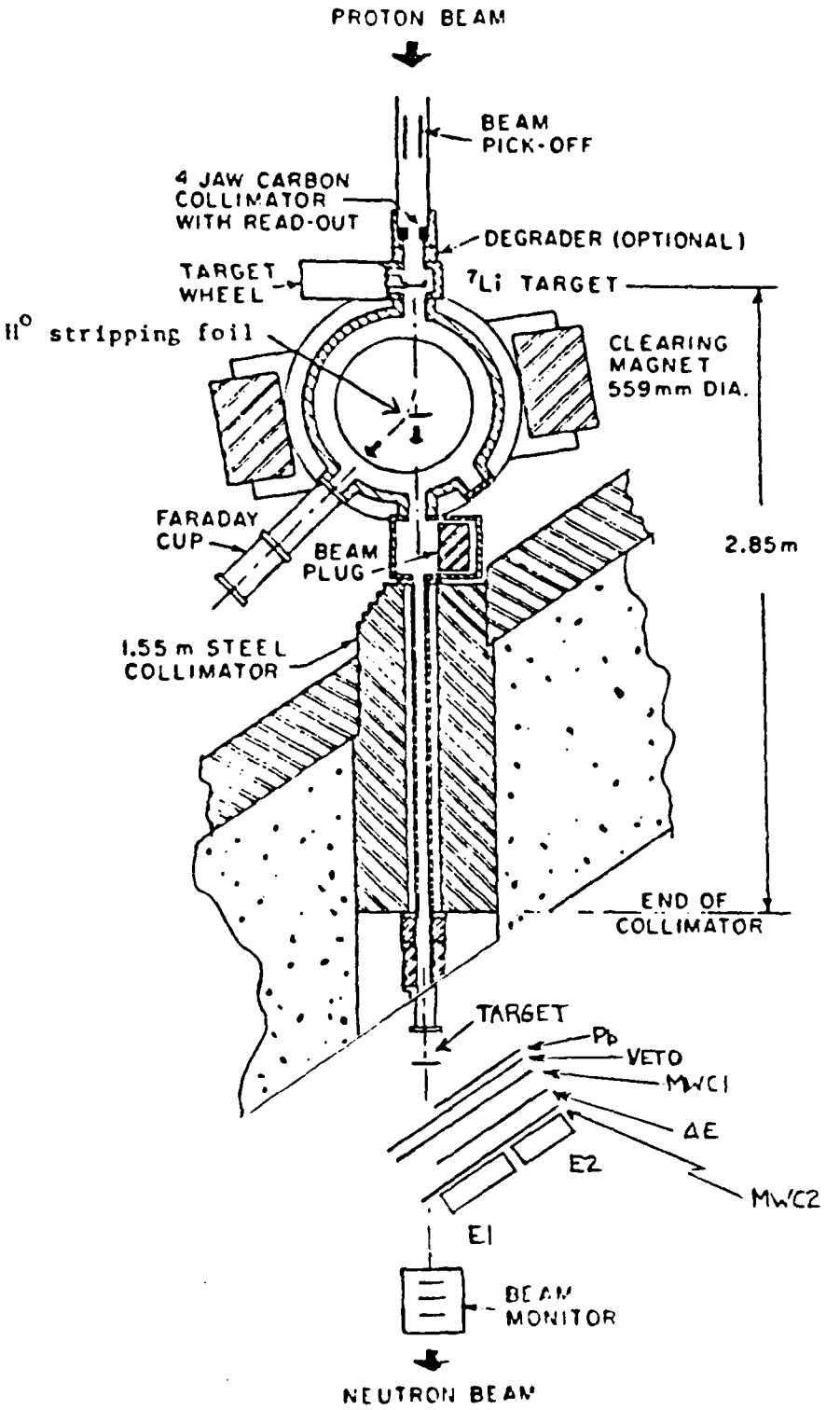

Figure 4

Neutron Beam Facility at Crocker Nuclear Lab.

still keep secondary collisions in the iron below 5%. The iron target, along with a carbon and CH_2 target (both used for calibration) were mounted on a ladder that could be lowered or raised remotely from outside the experimental area.

Since only a small portion of the neutrons will react with the target, the majority continue through the system to the neutron monitor subsystem (next section) and no longer interact with the system. Those that do strike the target but scatter outside an 8 to 42 degree range again will be eliminated due to an actual physical loss to the system, or, by further coincidence cuts to be explained later. Neutrons within the resultant "window" of 8 to 42 degrees, by system geometry, continue on to the veto sub-system for further acquisition.

The Neutron Monitor

The neutron monitor (see figure[15] 5), located 7 meters from the production target oversees the neutron beam intensity after it has exited the collimator and passed through the target. Using a method similar to that of the experiment, it vetos charged particles and then detects neutrons that are produced at a small CH_2 converter. A valid event is recorded when a proton successfully passes through counter B1 and B2 in coincidence.[16] The neutron monitor data is used as a check to insure the beam energy, intensity and peak shape is held constant during the course of the run.

The Veto

The proper operation of the veto subsystem is one of the most essential aspects of the laboratory set-up. The experiment hinges on

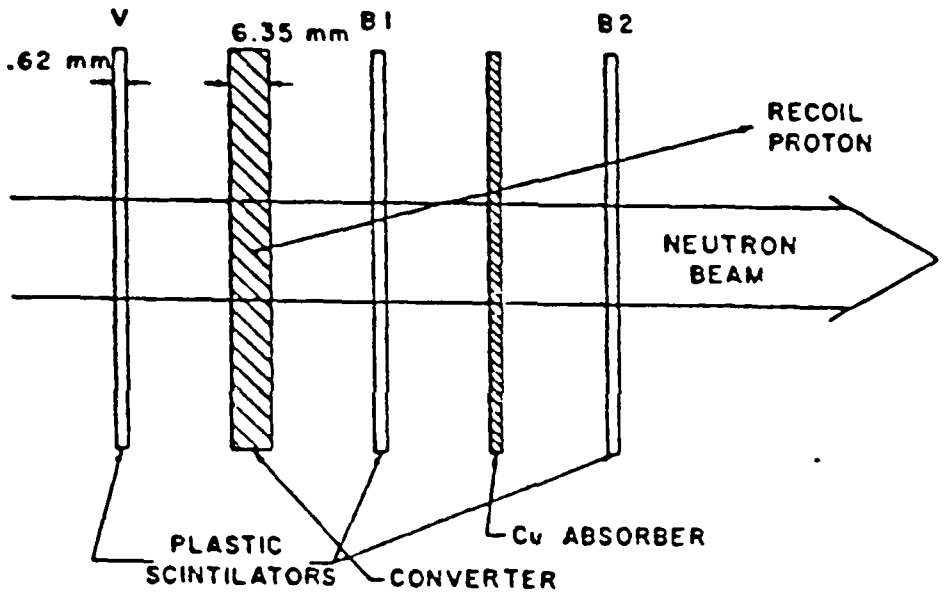

Figure 5

Diagram of the Neutron Beam Intensity Monitor.

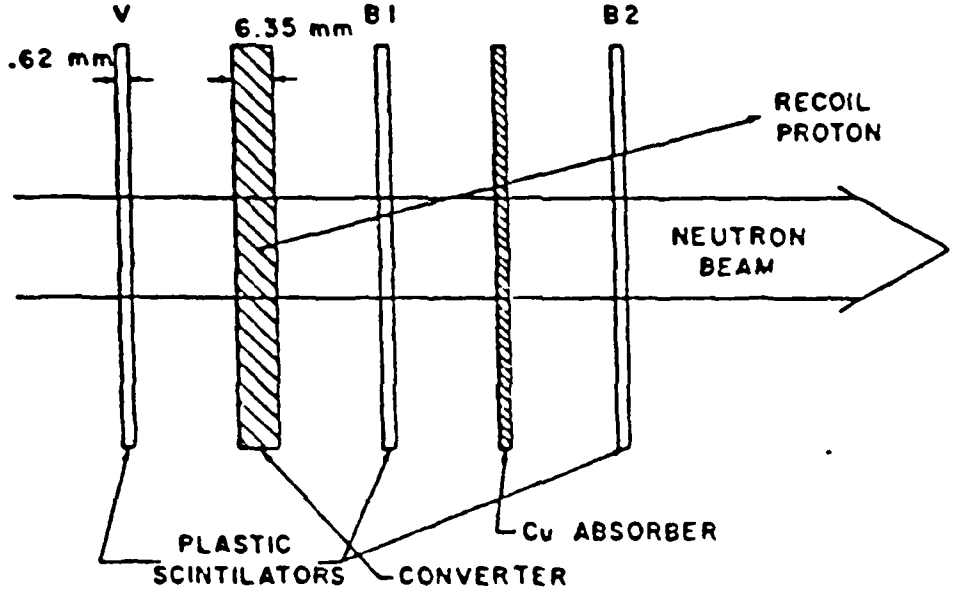

Figure 5

Diagram of the Neutron Beam Intensity Monitor.

the fact that unwanted scattered protons are eliminated from the system and that all hadron reactions, from the veto subsystem on, are only caused by neutrons.

The veto subsystem is in anticoincidence with the other detectors and eliminates a charged particle (proton, electron) signal by negating the coincidence signal between Wire Chamber One (WC1), ΔE, and Detector E One (E1). (See figure 6.)

Because of the importance of the veto subsystem, extensive tests were made by use of a H^{o} beam from the cyclotron. The beam was directed through a thin plastic detector, the Veto MWC and E1 with the Veto in anticoincidence with the other two detectors. With the Veto off, a measurement was made of events per unit time. The Veto was then turned on and a second measurement of events was made. Evaluating the results showed the Veto's effectiveness to be at least 99.7%. But this was not sufficient for the experiment, and, it was therefore decided that a ¼ inch lead degrader should be added to the system in front of the Veto MWC (see figure 6). With the addition of this degrader the protons passing through the system, [from Fe(n,p'x)], would be stopped or slowed to energies which were not of interest. Calculations demonstrated that the addition of the lead sheet only attenuated neutrons by a factor of 3% while effectively making the overall veto subsystem efficiency virtually 100%.

Due to the importance of the Veto, tests were made throughout the experiment to insure continued optimal performance.

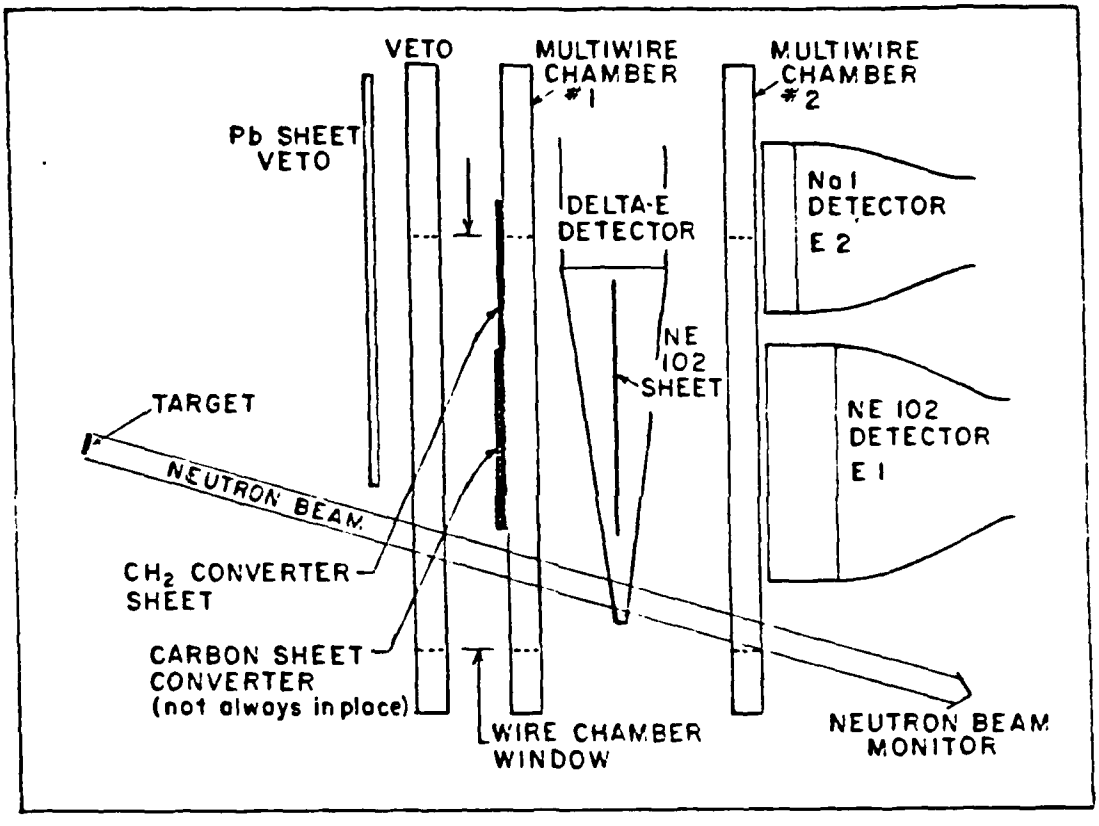

Figure 6

Top view of the (n,n'x) Detection Facility.

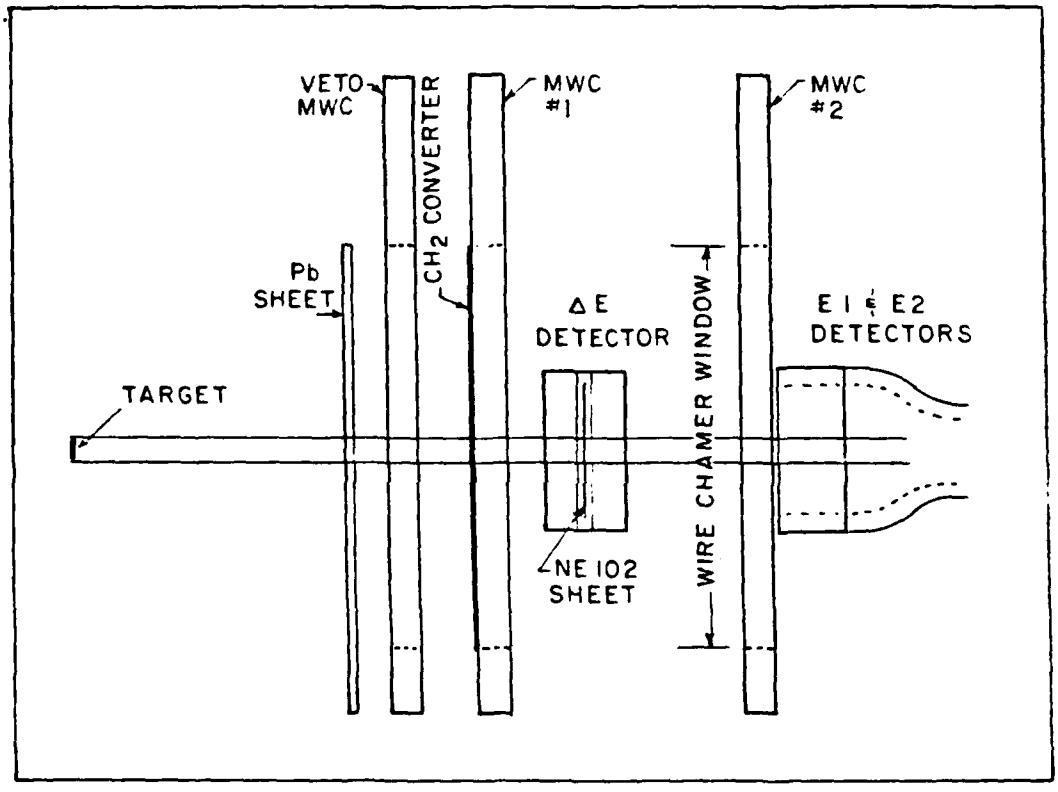

Figure 7

Side view of the (n,n'x) Detection Facility.

The Polyethylene (CH_2) Converter

The only particles still in coincidence, and therefore being tracked by the system after passing through the Veto, are the scattered neutrons. After traveling through 4 cm of air, they are now incident on a CH_2 converter, [.076 cm thick (.075g/cm^2)], mounted across the face of MWC1 (see figure 6) thirty cm from the Fe target. A percentage of these neutrons interact with the CH_2 and produce recoil protons. These protons are then tracked as charged particles (protons) passing through the rest of the experimental system. At this point, the system loses track of the neutrons that don't interact with the CH_2. This loss will be corrected for in the computer analysis phase as discussed later.

The Multi-Wire Chamber Detectors

The Multi-Wire Chambers and the Veto chamber, discussed earlier, are constructed and function identically. Each consists of four layers of Al framing sandwiched together providing a 30 cm square reaction window which is covered on each side with aluminized mylar. In between the sandwiching is one anode net plane with wires 2 mm apart and two cathode wire-net planes each having wires 1 mm apart.[17]

To maintain a uniform electric field between the wire planes "Magic Gas", consisting of 72% argon, 23.5% isobutane, 4% methylal, and .5% freon constantly flows between the wire planes. When a particle passes through the MWC, some of the gas is ionized producing free electrons. These electrons are accelerated toward the anode wires and an avalanche of electrons are formed by the ionization produced by the primary electrons. When all of these electrons strike the MWC wires, a signal is created that is used for analysis. The freon, which easily reacts

with the electrons, prevents the production of multiple signal events by reducing the mean free path of the charged particles. The methylal combines with the resultant ions that collect around the cathode plane. The constant flow of magic gas flushes out of the wire chamber freeing the wire planes from interference.

From each MWC there are four signals, each delayed by differing amounts of time depending on the location of the particles impact. These signals are discriminated, time digitized and processed by computer giving the X and Y coordinates of the impact on the detector plane. Accuracy in the X direction has been measured within 1 mm and that in the Y direction is measured to about 2 mm.

A proton emerging from the converter immediately passes through MWC1 (see figure 6) where its strike coordinate is processed through the data acquisition computer program and recorded as the proton continues toward the ΔE.

The ΔE Detector and MWC2

The ΔE detector used in the experiment has a .1 cm thick NE102 plastic scintillator 10 cm high and 18.7 cm long. The scintillator was connected to a light pipe which was in turn connected to a 7.6 cm diameter photomultiplier tube. Over the scintillator was a tapered tent of aluminum inside and aluminized mylar outside to assist in photon collection (see figure 6). Each time a ΔE-E or ΔE-E-MWC coincidence was recorded, the ΔE signal was sent to the acquisition computer and recorded along with the E and MWC signals. (Through analysis of its energy loss signal for a given E, it is determined whether the particle was a proton, deuteron or gamma ray: see Analysis section for

explanation of how cuts were made.) After going through the ΔE the particle passes through approximately 5 cm of air to be sensed in MWC2, where again, its strike coordinate is processed and recorded as the particle enters the area where E1 and E2 are located.

E1 and E2 Detectors

The two E detectors, located directly behind MWC2, give the maximum angular range possible for the wire chamber set-up. E1 is a 12.7 cm by 17.78 cm NE102 plastic scintillator, 5 cm thick, connected to a light pipe which was in turn connected to a 12.7 cm photomultiplier (see figure 6). E2 is 12.7 cm circular NaI detector, 1.9 cm thick, again with a 12.7 cm photomultiplier tube. Both E detectors are in coincidence with the ΔE and MWC1.

Since the particle loses all of its kinetic energy when it strikes the detectors, the magnitude of this loss is measured by the number of photons created in the scintillator. Thus the detector serves a dual purpose by producing a magnitude E and coincidence signal.

Data Acquisition and Processing

As mentioned in the introduction, for every beam burst, a TOF signal is created by measuring the time of MWC1-ΔE-E1 or E2 coincidence relative to the Beam Pickoff signal. This Beam Pickoff signal is the one produced upstream of the Li target due to protons in the main peak. This information forms an acquisition event with the impact position information from the MWC's and signals from E1, or E2, and ΔE. These signals from the experimental area (see figure 8) are all sent to the counting room by means of low attenuation cables.

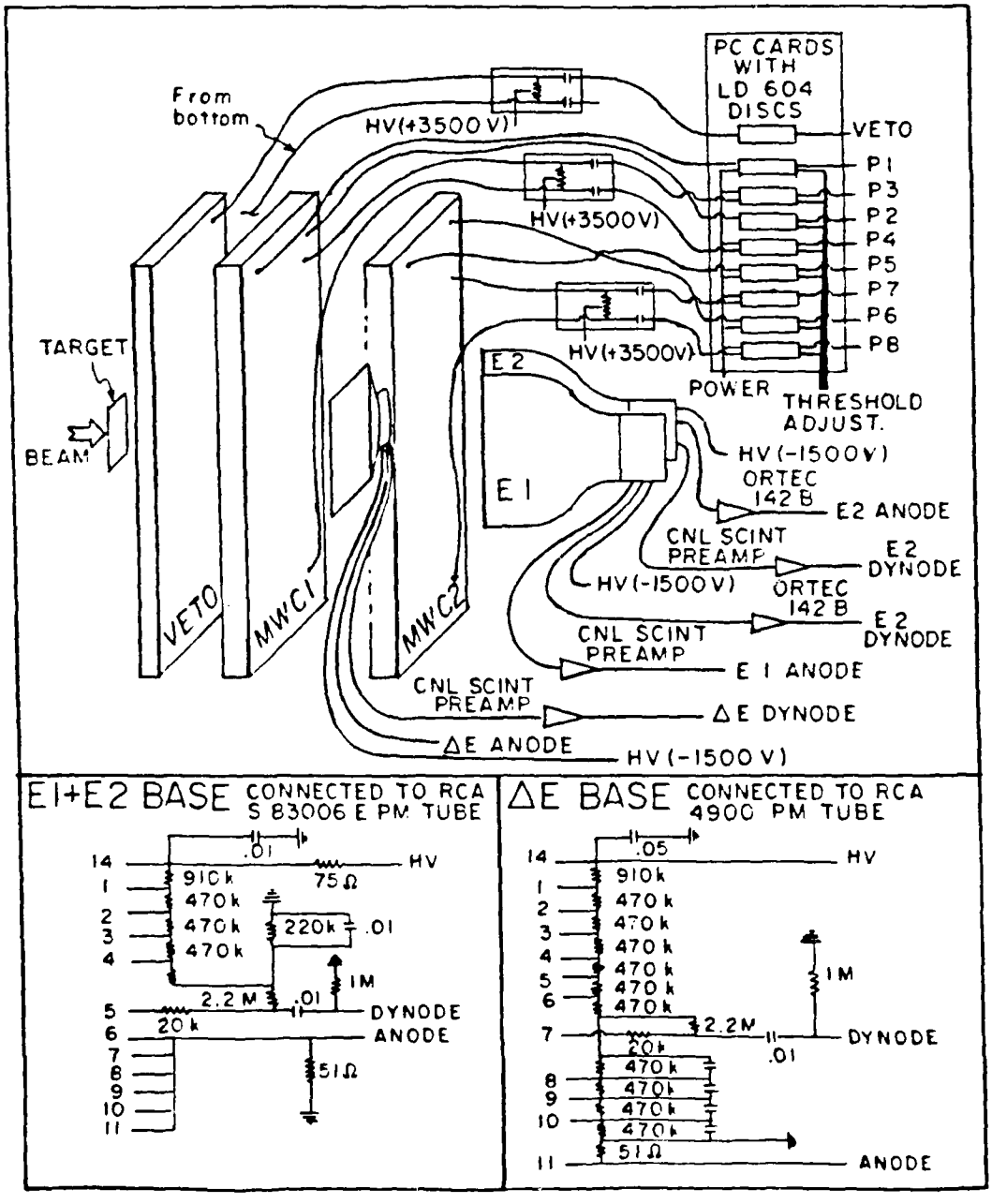

Figure 8

Basic wiring diagram for the (n,n'x) experimental area.

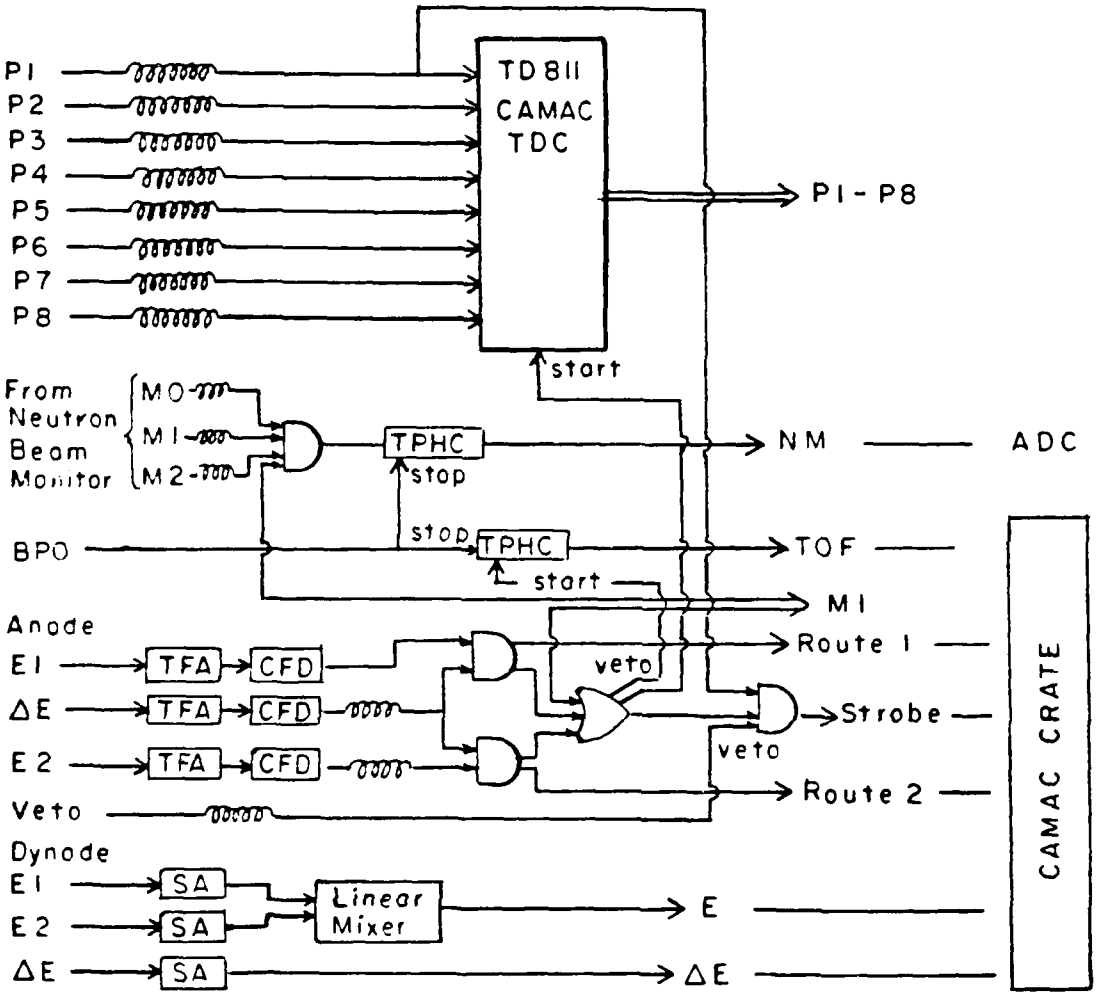

LEGEND: TPHC = TIME TO PULSE HEIGHT CONVERTER
TFA = TIMING FILTER AMPLIFIER
LFD = CONSTANT FRACTION DISCRIMINATOR
SA = SPECTROSCOPIC AMPLIFIER
MI = MASTER INHIBIT

Figure 9

Counting room wiring diagram for acquisition.

PART V

FINAL ANALYSIS, RESULTS AND DISCUSSION

Overview

As the experiment was originally envisioned, data was to be analyzed from 4 to 32 degrees. However, fewer counts than expected were acquired in detector E2 (covering angles 26 to 32 degrees), thereby making an accurate energy calibration and further analysis impossible for this detector.

In the low angle range, two problems made the analysis very difficult. The much larger than expected carbon contamination of the spectra (due to the CH_2, as already explained) and the multiple scattering in the system caused a disproportionate number of counts in the elastic and the (n,n'x) continuum regions of the energy spectrum. Since different thicknesses of Fe targets had not been run, correction factors for the multiple scattering could not be accurately calculated. Because of the two problems it was decided to concentrate on the mid-angle region, (14 to 24 degrees), where multiple scattering and the carbon spectra had little or no effect, and statistics were acceptable.

This experiment represents the first concerted effort to measure the angle dependent elastic and (n,n'x) inelastic cross sections for a nucleus over a wide energy range. The lack of prior experimental data makes comparisons to accepted values impossible. Therefore, in the balance of this section, the results presented on elastic and (n,n'x) scattering will be compared to either theoretical predictions and/or the experimental results due to (p,p'x) reactions. Systematic and

However, the ratio of the energy dependence of attenuation $A_1(\text{non-el})/A_1(\text{el})$ has at most a 3% effect for the nuclei involved in this experiment. Therefore, the value for the continuum cross section can be reduced to

$$\sigma(\text{non-el}) = N_{Fe}(\text{non-el})\sigma_{Fe}(\text{el})/N_{Fe}(\text{el}). \qquad [26]$$

The methods and corrections described above constitute the basis for arriving at the results about to be discussed. Improvements to the analysis steps for similar experiments to follow will be discussed in the last section of the paper.

Energy Calibration with a Carbon Target

To calibrate detectors E1 and E2, several runs were made using a carbon target instead of the Fe target, in the absence of the Veto. Neutrons incident on this carbon target produced very discrete, easy to identify, energy spectrum peaks [due to $^{12}C(n,p)^{12}B$ transitions to the groundstate, giant dipole etc.]. A channel in the energy spectrum was associated with each of the ^{12}B main excitation peaks at 0.0, 4.4, and 7.7 MeV and a linear regression calculated. The results were then used to calibrate all energy spectra calculations during the rest of the analysis.

Cross Section Calibration with a CH_2 Target

Accurately determining the (n,n'x) cross section for ^{56}Fe involves comparing experimental results with those predicted by the Optical Model for Fe and the experimental angle being evaluated.

We know from equation [23] that our theoretical values are

$$N_{Fe}^{CH_2} = N_{Fe}(\text{elastic}) = I_F \; A_0^F \, \sigma(el) w A_1^F(el)$$

or $$N_{Fe}(\text{elastic}) = k\sigma_{Fe}(el)A_1^F(\varepsilon_0). \qquad [24]$$

Using the U.C. Vax System "DWUCK" optical model program, the theoretical elastic cross section for equation [24] can be calculated. Similarly, for the continuum the non-elastic equivalent for [24] can be calculated as

$$N_{Fe}^{H_2}(\text{non-el}) = k\sigma_{Fe}(\text{non-el})A_1^F. \qquad [25]$$

Combining equation [24] and [25] results in

$$N_{Fe}(\text{non-el})/N_{Fe}(el) = \sigma_{Fe}(n,n'x)A_1(\text{non-el})/\sigma_{Fe}(el)A_1(el).$$

Calibration of Detectors

For all the detectors, ΔE, E1 and E2, the response varies across the detector face reference the impact position of the impinging particle. As a result, each detector surface was mapped, by square centimeter intervals, using a radioactive source or by the H° beam from the cyclotron. This data on the light response was then normalized, kept on file, and used by the computer during program execution to correct for non-uniform response during the analysis phase.

Loss of Energy by Recoil Protons

Whenever a charged particle passes through a media; it loses energy at a rate dependent on its energy and the composition of the media. This property must be, and is, accounted for in the analysis steps. Mean energy loss thru each material (*air, aluminum foil, mylar etc.*) was calculated by the program "TFPACK". The program stored this energy loss data and added it to the energy detected for each proton by E1 and E2. This "true" proton energy was then used for all further calculations.

Multi-Wire Chamber Calibration

There is a slight variation in MWC response across the wire planes when finding the X and Y coordinate for the passing point of a charged particle. To correct for this, a collimated ^{55}Fe source was used for calibration, and by analysis, a linear fit was made for each of the wire chambers in the X and Y directions to be used for position analysis during the actual run.

$$N^C = I_F^C A_o^F n_{Fe} \sigma_{Fe} w_C A_1^C (\varepsilon^C + \varepsilon') \cong B^C(\varepsilon^C + \varepsilon') \qquad [21]$$

where $\varepsilon^C = k_C n_C^C$.

But again the background effects must be taken into account. This by analogy results in an equation similar in form to [19].

$$N_{Fe}^C = N_F^C - .84\ IN_E \qquad [22]$$

where $I = I_F^C / I_E^C$

or $N_{Fe}^C = FECC - .84CC.$

To determine the counts caused by the neutron interaction with the target and the n' with the hydrogen of the converter, equation [22] must be subtracted from equation [20]. This subtraction must be properly weighted for the number of dumps and relative thicknesses of carbon for each type run. Since the two different converters were placed in the identical position for each type run $w^{CH_2} = w^C$.

Therefore, $N_{Fe}^{H_2} = B^{CH_2}(\varepsilon^{CH_2} + \varepsilon') - B^C InA(\varepsilon_C^C + \varepsilon') \qquad [23]$

where $I = I_F^{CH_2} / I_F^C$,

$n = n^{CH_2} / n_C^C$ and

$A = A^{CH_2} / A_1^C$.

This can be rewritten as

(FE-EMPTY) - (FECC-CC) = the real (n,n'x) spectrum.

Along with the background effects explained above, there is also a possibility that upon striking the CH_2 converter the recoil neutron will react with the carbon atom, rather than the hydrogen. To correct for these carbon interactions, a thin carbon sheet was used as a converter for a series of runs, both with the target in place (FECC), and without the target (CC).

In previous experiments, where (p,n) spectra were measured, it had been found that the carbon in the CH_2 had at most a 5% background effect on neutron energies of 60 MeV.[23] However in this experiment, it was found this figure to be true only in the elastic peak region. In the inelastic continuum, the contribution, due to the large number of elastic neutrons striking the carbon, was approximately 40% at forward angles and decreased in percentage as the scattering angle increased. Due to this factor, extra care had to be taken in choosing the proton cuts and finding the proper method to subtract the carbon events.

The equations for the net counts due to the iron target and CH_2 converter can be defined as

$$N^{CH_2} = I_p A_0^F n_{Fe} \sigma_{Fe} w_{CH_2} A_1^{CH_2} (\varepsilon^{CH_2} + \varepsilon') \cong B^{CH_2} (\varepsilon^{CH_2} + \varepsilon') \qquad [20]$$

where ε' = conversions produced due to material effects other than the CH_2 converter and

$$\varepsilon^{CH_2} = \varepsilon_H^{CH_2} + \varepsilon_L^{CH_2} = k_H n_H^{CH_2} + k_C n_C^{CH_2} .$$

Since the attenuation for both converters is small and approximately the same, the equation for the carbon converter net counts is defined by

$$N_{Fe}^{CH_2} = N_F^{CH_2} - (wf)N_E \qquad [18]$$

where $N_F^{CH_2} = IA\,(n\,\sigma)w\,A,$

$$wf = IA^F\,A_1^F/A_0^E\,A_1^E \text{ and}$$

$$I = I_F^{CH_2}/I_E^{CH_2}$$

$A_0^F A_1^F/A_0^E A_1^E$ can be simplified realizing that the difference can be approximated by $e^{-\sigma n}$ where

n = [density of Fe target (g/cm^2)][A_v)/Atomic weight of Fe.

A good approximation, neglecting E dependence, for the average cross section for iron is 2 barns. Using this value results in the final equation for the empty target subtraction of

$$N_{Fe}^{CH_2} = N_F^{CH_2} - .84(I)N_E^{FN} \qquad [19]$$

or $N_{Fe}^{CH_2} = FE - .84I(EMPTY)$

It becomes clear that the effects of the attenuation in iron is to overly increase the background effect. This result is corrected for by use of the .84 weight factor. This attenuation effect would have an E dependence that would have a greater effect in the low energy part of the spectrum since these particles are the ones attenuated the most. This effect however was calculated at less than 3% over the entire energy spectrum. It is approximately counterbalanced by the loss of counts due to nuclear interactions taking place in the scintillator of E1 and E2. This loss of counts varies from 5% (at 65 MeV) to 1% (at 25 MeV) over the energy spectrum.

EMPTY runs). These events are subtracted from the target runs (FE) during final analysis.

In order to calculate the proper subtraction, the following equation for the number of counts due to the iron target and CH_2 converter was used.[22]

$$N_F^{CH_2} = I_F^{CH_2} (n_{Fe}\,\sigma_{Fe} + n_A\,\sigma_A) w_{CH_2}\, A_0^F(E_0)(\varepsilon^{CH_2} + \varepsilon') \qquad [16]$$

where A_0^I = attenuation of beam due to ½ thickness of Fe,

$I_F^{CH_2}$ = neutron beam intensity (dumps) with target and CH_2 converter,

$n_A\sigma$ = neutron scattering from materials other than Fe,

$n_{Fe}\sigma_{Fe}$ = neutron scattering from Fe,

w_{CH_2} = solid angle of given angular slice for scattered neutrons striking the converter,

$A_0^F(E')$ = attenuation for outgoing neutron through ½ thickness of Fe, lead, air, etc,

ε^{CH_2} = the efficiency for converting to protons from neutrons, and

ε' = conversion that takes place other than in the CH_2 converter from sources such as the windows, air, etc.

And by analogy the equation for target empty that accounts for the air windows, etc., would be

$$N_F^{CH_2} = I_E^{CH_2}\, A_0^E\, (n_E\sigma_E) w_{CH_2}\, A_1^E(E')(\varepsilon^{CH_2} + \varepsilon') \qquad [17]$$

Solving equations [16] and [17] for $n\sigma$ and equating the resulting terms produces

However before this information is recorded, a loss of events must be accounted for due to protons, within the allowed angle of conversion, actually missing the detector system causing the raw (n,p) count rate to far underestimate the actual number allowed (n,p) reactions for the system. By use of Binstocks' parametrization of differential (n,p) cross sections for incident neutron energies between 25-100 MeV[21] and the energy of the recoil neutron E_n, as calculated above, allows the computer to calculate the proper cross section per event; and multiply the raw count in each bin by the proper weighting factor. This produces a $\frac{d^2\sigma}{dEd\Omega}$ for further analysis. (A record of real count data is also maintained so the statistical error of the spectra produced can be calculated.) With the single neutron event analysis complete, the computer separates the event into designated angular bins and energy channels.

The above simplified view of the overall method can only be made to produce satisfactory results if corrections are made in several areas of processing and calibration.

Elimination of Events not caused by n' interaction with H in the Converter

Whenever the cyclotron is functioning, there is a normal background of particles coming from various sources such as the beam halo, the Faraday Cup (located near the experimental area), gamma rays produced in the beam line, protons produced in MWC windows, and ricochets of particles from all sources. In order to account for these events, runs were made at various times with the CH_2 converter, but no target (called

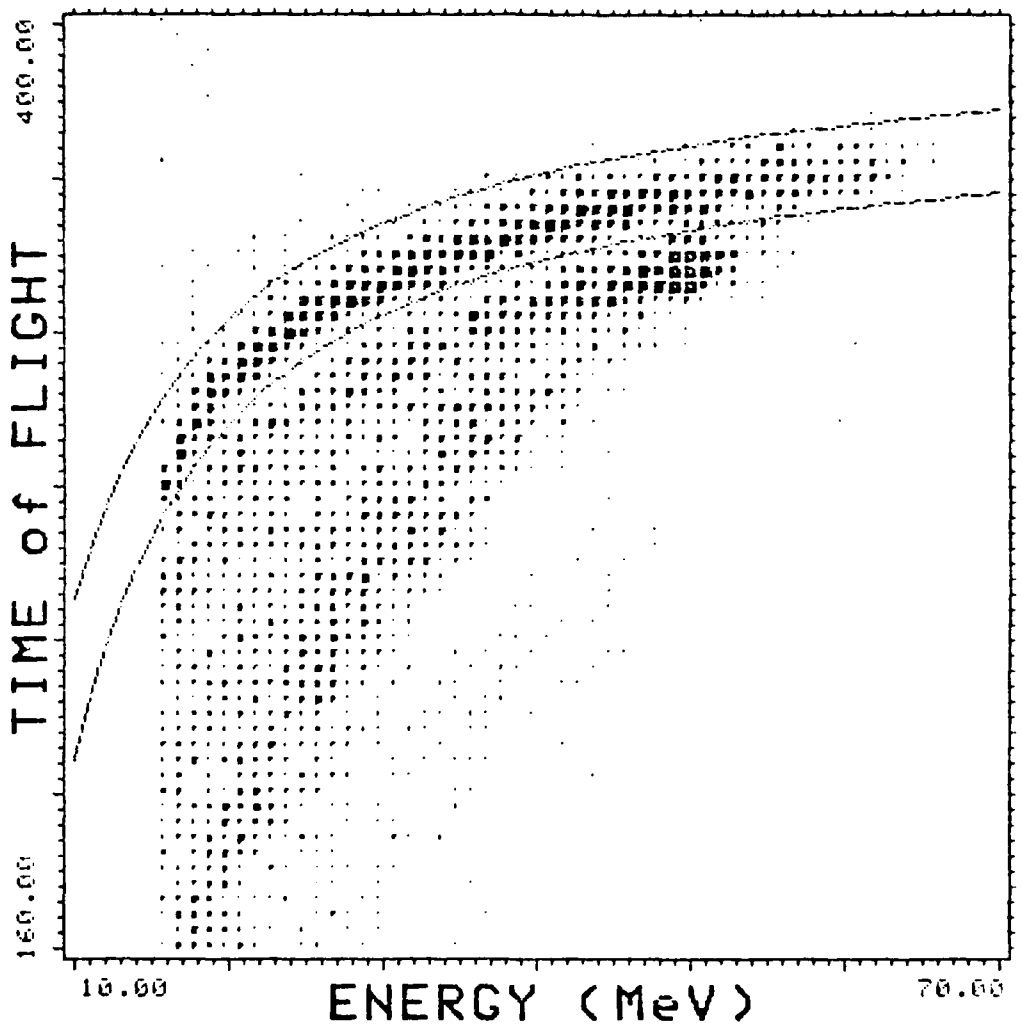

Figure 11

Software cuts used for the E-TOF matrix array.

the uncertainty discussion for more details.) By properly defining the "window" cuts, desired proton events can be isolated from all others (solid lines represent cuts).

New Lilgan also separates the unwanted, beam non-peak events, from those beam peak events needed for analysis. A neutron TOF vs Energy array of data using the TOF and E signal from the runs is produced by the program (see figure 11). Cuts are again made, as shown in the figure, to eliminate the events produced by the neutron tail from further analysis. The remaining events are caused by n' interaction with the hydrogen and carbon in the converter (carbon reaction separation will be explained later).

Using these TOF and proton windows created in "Lilgan", the main analysis program, "TFPACK" takes the two x-y data points recorded from the MWC's and calculates the trajectory, and therefore the proton's starting point at the converter. With knowledge of this starting point, the angle the recoil neutron has to take from the target is then calculated.

From the data recorded from E1 and E2, the proton's energy at the end of our system (E_p) is known and is corrected for energy losses through the system. Assuming n' comes from the target, then the angle θ, which was calculated above, is non-relativistically related to E_n, the energy of the scattered neutron from the target, by $E_n = E_p/\mathrm{Cos}^2\theta$.[20] (A relativistic correction would only result in a change of energy of a few percent. This correction is very small considering the other energy uncertainties and so is neglected.) Overall then, the angle and energy of the recoil neutron has been determined.

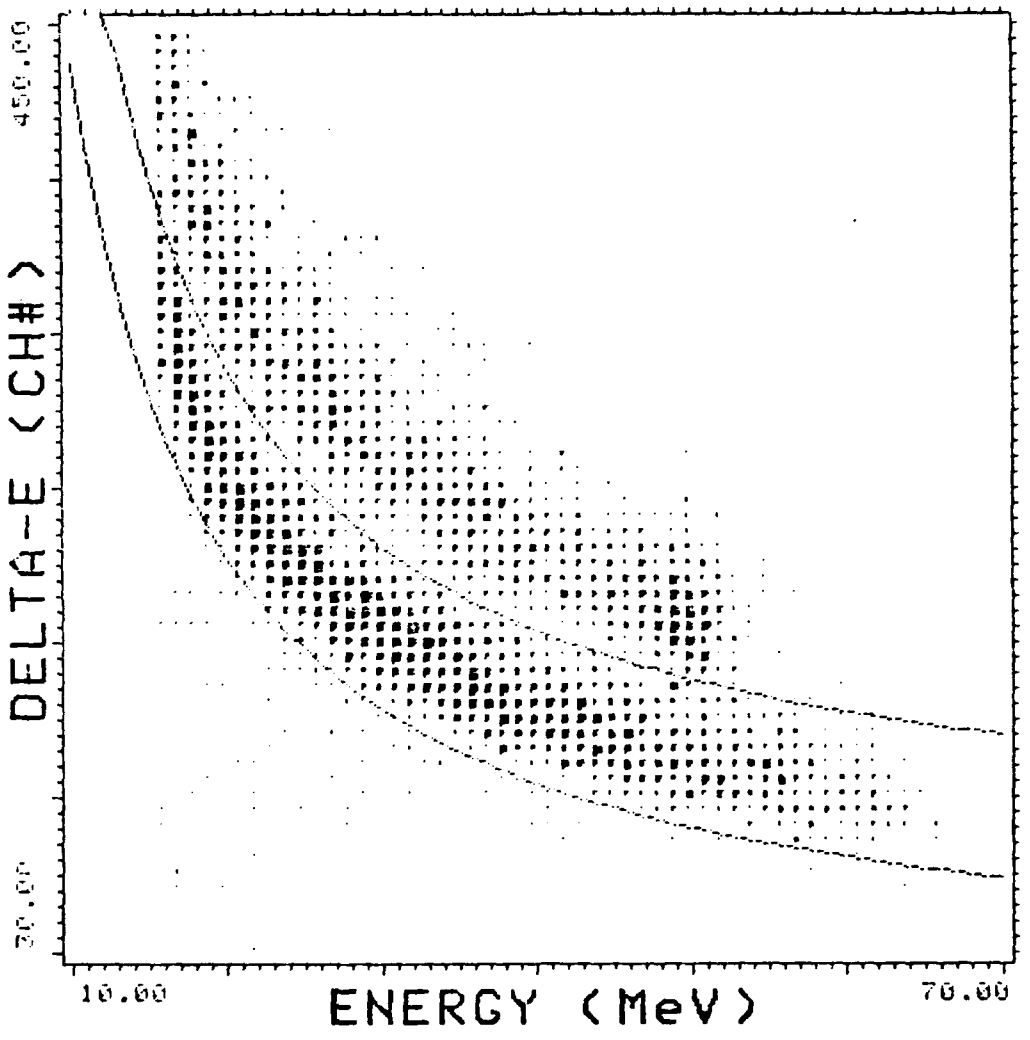

Figure 10

Software cuts used for the E-ΔE matrix array.

PART IV

METHODOLOGY OF DATA ANALYSIS

With an understanding of the setup, the basic experimental analysis method can be easily followed. This analysis method is similar to the general analysis method used for the prototype (n,n'x) run made in 1981.[19] In almost all cases the methodology was proven valid and with minor modifications as explained here. Corrections needed for the method will be explained in detail later in this section.

As already explained, a neutron (produced by $^{7}Li(p,n)$) strikes the Fe target. When neutrons from the Fe(n,n'x) strike the CH_2 converter and react with the nuclei (elastically or inelastically), a proton may be ejected from the CH_2. This "recoil" proton then passes thru the detector system where data is recorded as it passes through the MWC's, ΔE, and when it is finally stopped in E1 or E2. The TOF signal (from the beam pickoff probe and coincidence of MWC1, ΔE and E1 or E2) is also stored with each of these event sets and used later to pick out the events caused by the beam peak only.

To analyze the raw data events, a CNL Neutron Group program called "New Lilgan" was used to separate the desired proton events after (n,p), from unwanted particles, such as deuterons, that were also produced in the conversion process. The software program produces a Change in Energy (ΔE) vs. Energy (E) array of data as shown in figure 10. This is accomplished by using the ΔE and E data recorded during the run for all particles falling within allowed conversion angles (0 to 15 degrees) for the (n,p) reaction at the converter. (It was found that larger allowed angular cuts resulted in energy resolutions that were unacceptable. See

In the counting room, electronic logic is used to determine if an event is valid. The anode signals from E1 and E2 (see figure 9) go through Timing Filter Amplifiers (TFA) and Constant Fraction Discriminators (CFD). They are then AND gated with the ΔE signal to create routes. These routes fan out with one leg joint to the CAMAC coincidence buffer and the other going through two AND/NOT gates (for veto's) first with the Master Inhibit (MI) and then with the Veto MWC. After successfully passing the AND/NOT gates a "Strobe" or event trigger is created. This strobe event passes through the CAMAC (Computer Aided Measurement and Control) branch driver system crate.[18] With this strobe anode signal the dynode intelligence carrying signal is allowed to pass into the TDC (Time Digital Converter) and ADC (Analog to Digital Converter) digitizing. The dynode digitized signal then passes to the CA 15 interface into the PDP 15/40 computer for on line processing and recording on a 7 track magnetic tape.

statistical errors, along with energy uncertainties, and their causes will also be explained in this section.

Elastic and (n,n'x) Continuum Results and Comparisons

The (n,n) Elastic Peak

Data for the elastic peak was analyzed in 2 degree bins from 14 to 24 degrees. A typical energy spectrum is shown in figure 12. The wide FWHM (5 MeV) on elastic peak is caused by the acceptance angle of the (n,p) reaction at the converter (as discussed in the Uncertainty Section below).

For the elastic peak, the theoretical normalization predictions for cross sections were based on the optical model (OM) equations of Bechetti and Greenless as calculated by version 01/07/78-DWUCK4 (Distorted Wave, U. of Colorado), as found in the U.C. VAX system. To normalize the elastic peak, the peak at 15 degrees was initially normalized to the optical model (OM) prediction for (n,n) at 65.5 MeV. Using this 15 degree value for the cross section, the other elastic peak cross sections were determined. As seen in figure 13, the shape of the (n,n) cross sections compare very favorably with the optical model predictions.

Since the results compared well with the OM, a renormalization was accomplished by using a combination of the OM and the (p,p'x) experimental data so as to more accurately portray the (n,n) results. First, the mean ratio between the (p,p) data and the (p,p) OM was found; this factor was multiplied by the OM prediction for (n,n) at 15 degrees. This new term at 15 degrees is the normalization factor that is used to

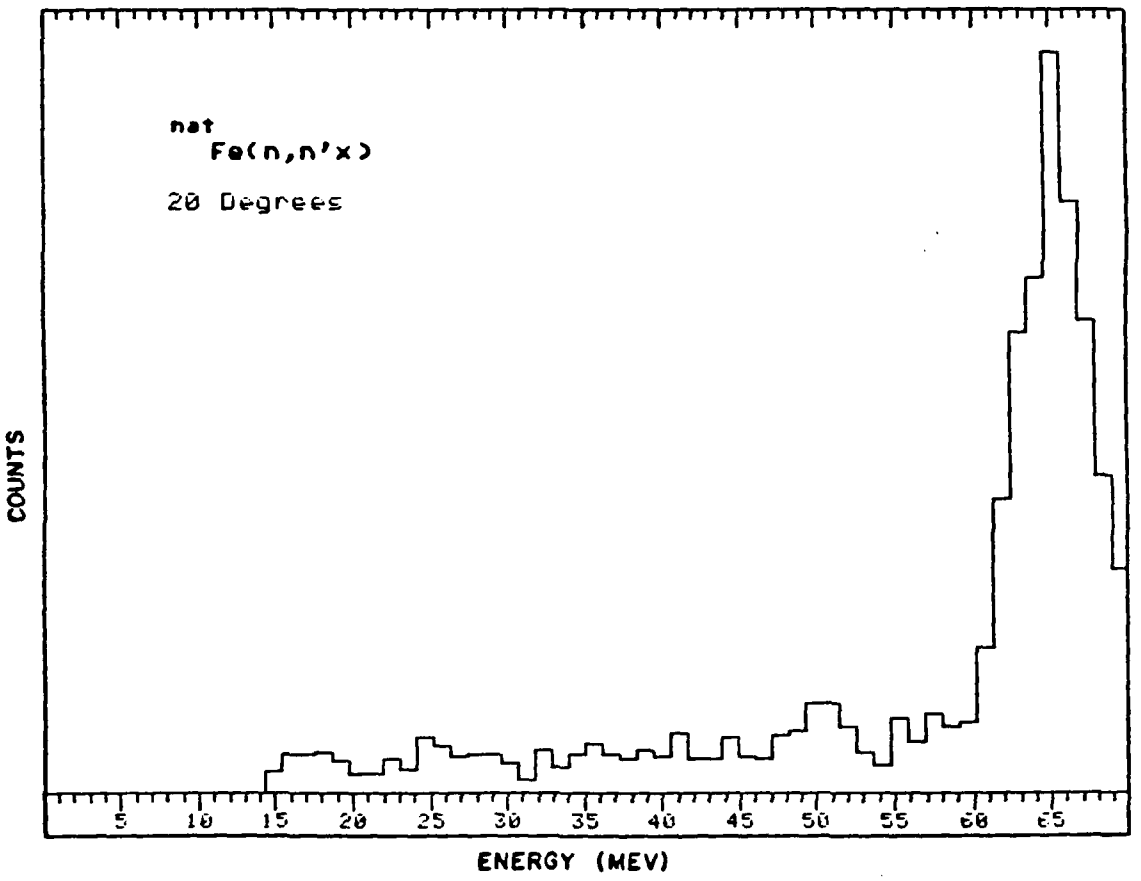

Figure 12

^{nat}Fe spectrum for (n,n'x) at 20 degrees.

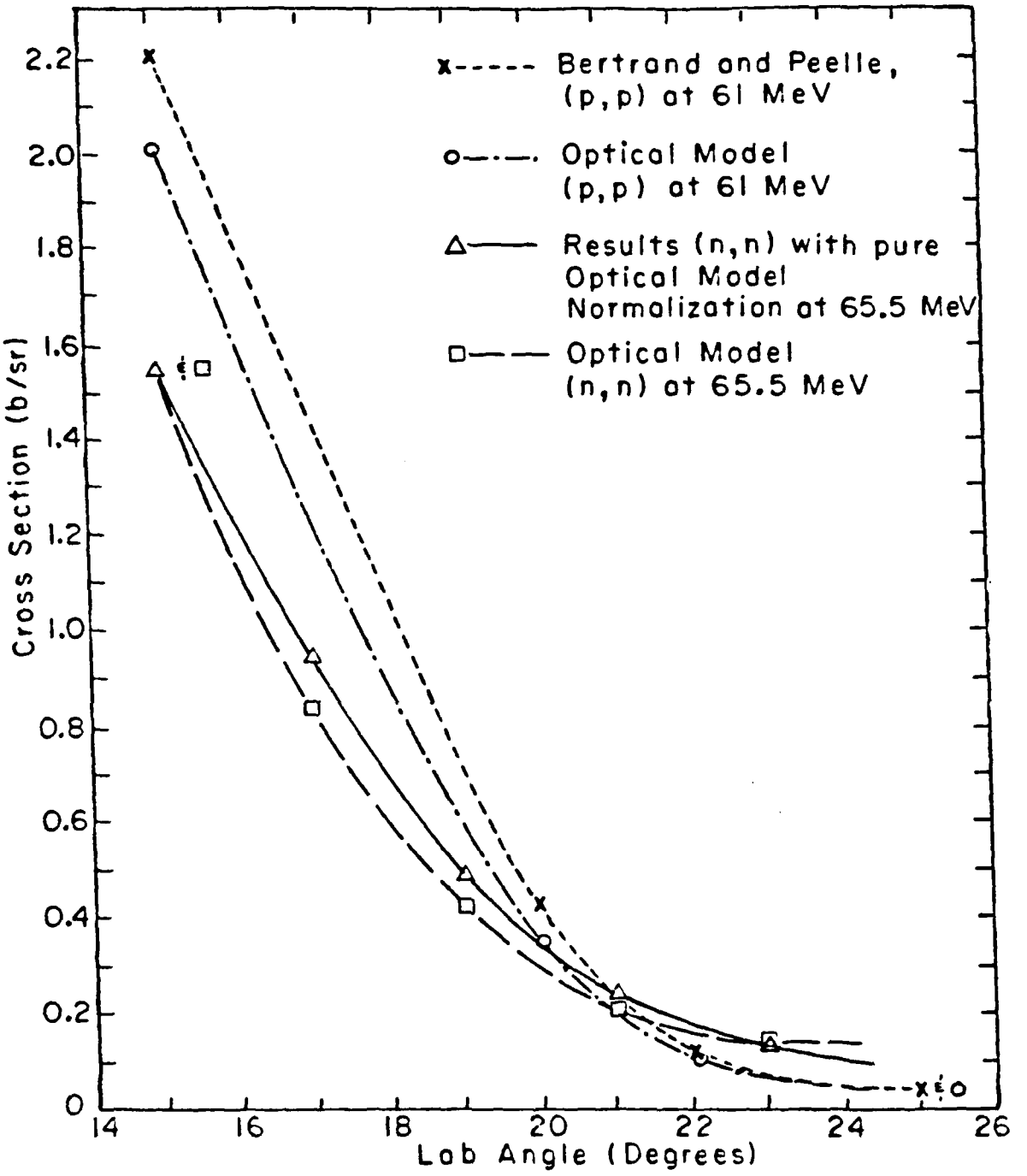

Figure 13

Initial (n,n) elastic peak normalization as compared to the OM prediction and (p,p) elastic peak data.

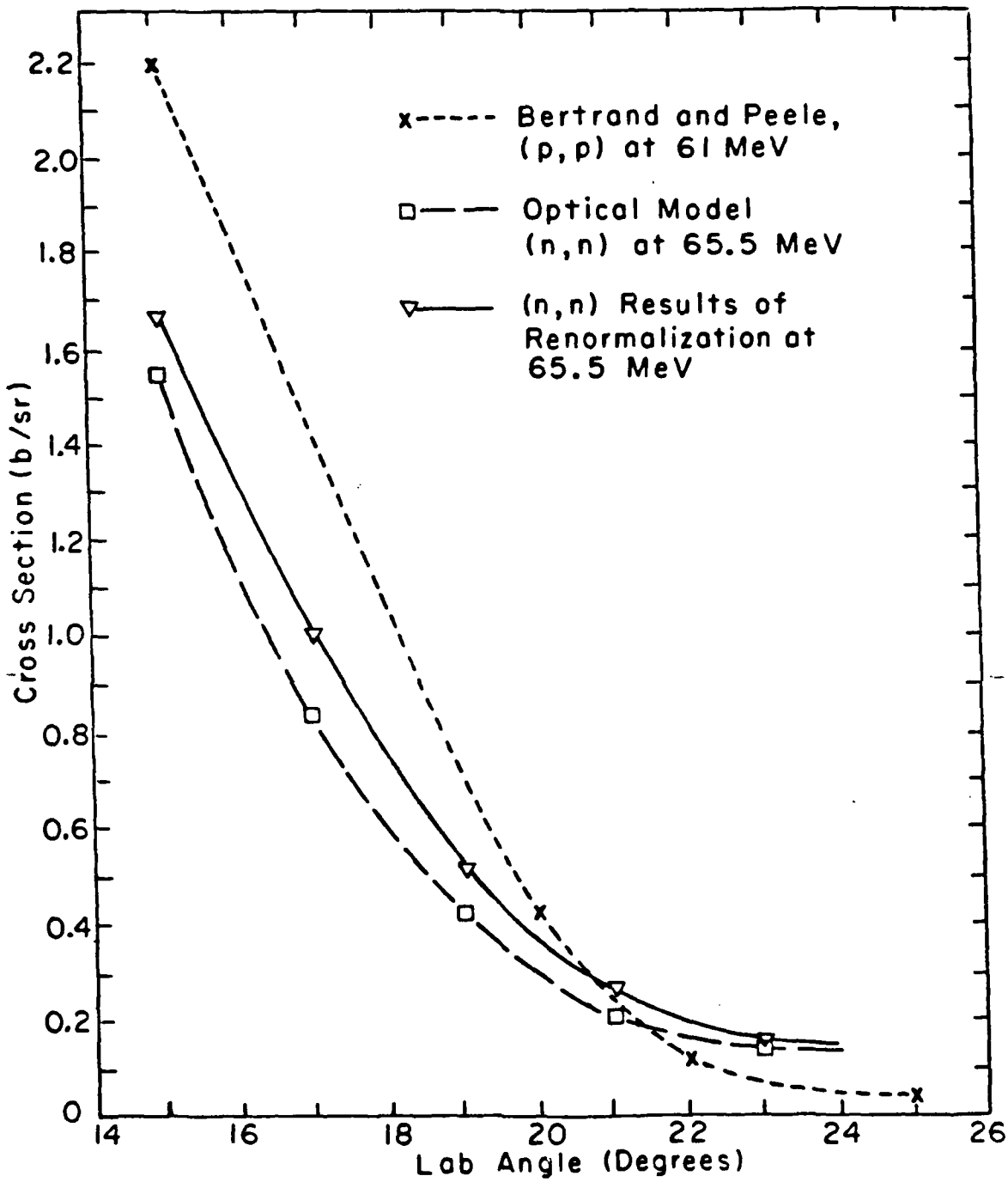

Figure 14

Final (n,n) elastic peak normalization as compared to the OM prediction and (p,p) elastic peak data.

find the cross sections for all other elastic peaks (see figure 14 and table 1). It should again be noted that the general magnitude and curve shape of the elastic peak cross section points are consistant with the OM prediction (as seen in figure 14). This new normalization cross section now becomes the basis for all cross section calculations, whether for the elastic or the continuum. Since it is an approximation, a systematic error of 7% will be attributed to this procedure.

The (n,n'x) Inelastic Continuum

For the target, energy range and angle used in this experiment, the most applicable proton data for comparison was found in the report "Tabulated Cross Sections for Hydrogen and Helium Particles produced by 61 MeV Protons on ^{56}Fe" by F.E. Bertrand and R.W. Peelle.[24] This report contained tabulated continuum cross sections/sr-MeV and elastic peak cross sections at various angles.

As already mentioned in the experimental methodology, the carbon contamination from the CH_2 converter had a much larger effect than expected for the experiment. This contamination only effected the results in the non-elastic region due to the C(n,p) Q value being approximately -13 MeV. Since this effect had not been predicted, beam time with the carbon converter was not sufficient for the statistics required for the carbon converter subtraction. After analysis of the carbon converter data, each angle bin for carbon above 12 degrees, had to be adjusted to eliminate extreme statistical inconsistencies before the weighted subtraction from the CH_2 converter runs. This smoothing process introduces an error beyond the statistical error calculated for each channel and is estimated between 2 and 9%.

TABLE 1

NORMALIZED CROSS SECTIONS FOR ELASTIC PEAKS

Lab Angle (degrees)	Normalized Cross Section (Lab) (b/sr)	Statistical Uncertainty (%)	Systematic Error (%)	O.M. (mb/sr)
15	1.66*	1.6	7.	1.54
17	1.00	1.9	7.	.841
19	.515	2.6	7.	.425
21	.260	3.8	7.	.222
23	.143	4.9	7.	.147

*Normalization Point.

The fully analyzed spectra for each two degree bin from 15 to 23 degrees is shown in figures 15 to 17. Also shown in Table 2 are the evaluated continuum cross sections for these spectra. In the lower bins, statistics are sufficient for general conclusions to be made, while the highest bin (23 degrees) is statistically unreliable.

Comparison of (p,p'x) to (n,n'x) Continuua at 20 degrees

As already mentioned in the Theory Section, a direct comparison of the (p,p'x) to (n,n'x) continuua cross sections should result in cross section ratios of approximately one.

The (p,p'x) continuum data of Bertrand and Peelle[25] were available at 20 degrees to make this comparison. Since there was no (n,n'x) angular bin centered at 20 degrees, the 19 and 21 degree bins were added together and the elastic peak result normalized for the proper cross section value. The (n,n'x) continuum cross section values were then calculated, put in 2 MeV bins and the results tabulated in table 3 and shown in figure 17. Also plotted are the (p,p'x) results of Bertrand and Peelle. It is immediately clear, even with the limited statistics for the (n,n'x) results, that the shape and cross sections for (n,n'x) are very similar in appearance and magnitude with the (p,p'x) results.

As a further indication of the similarity of the data, the energy integrated cross sections for the neutron and proton data was calculated. This resulted in a value of 139.6 mb/sr (±18 mb/sr) vs 138.2 mb/sr (±1.5 mb/sr) for (n,n'x) and (p,p'x) respectively. This close result again is consistent with our expected continuum ratio of .93 between the neutron and proton data as calculated in the theory

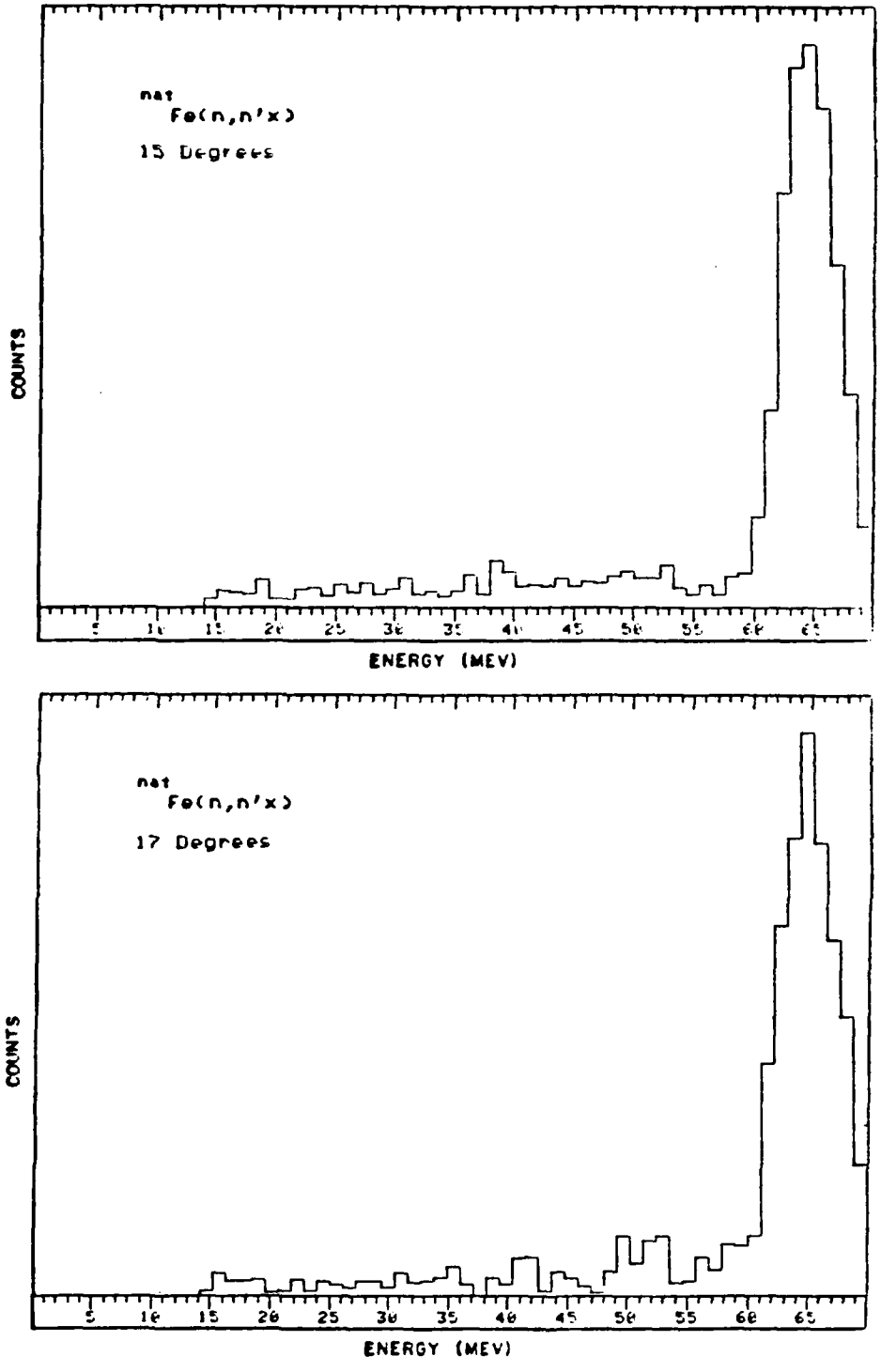

Figure 15

Fully analyzed (n,n'x) spectra from 14 to 18 degrees.

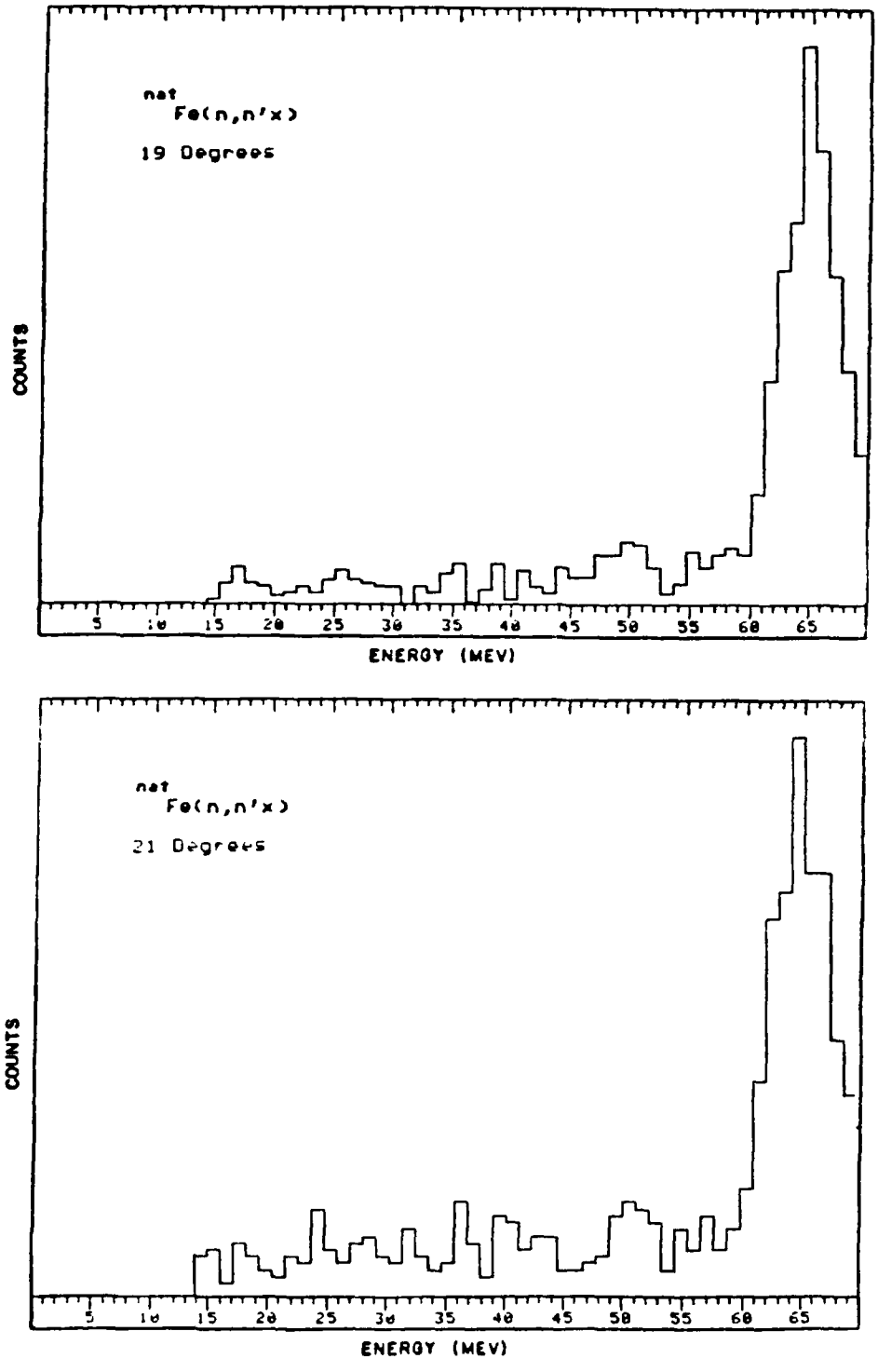

Figure 16

Fully analyzed (n,n'x) spectra from 18 to 22 degrees.

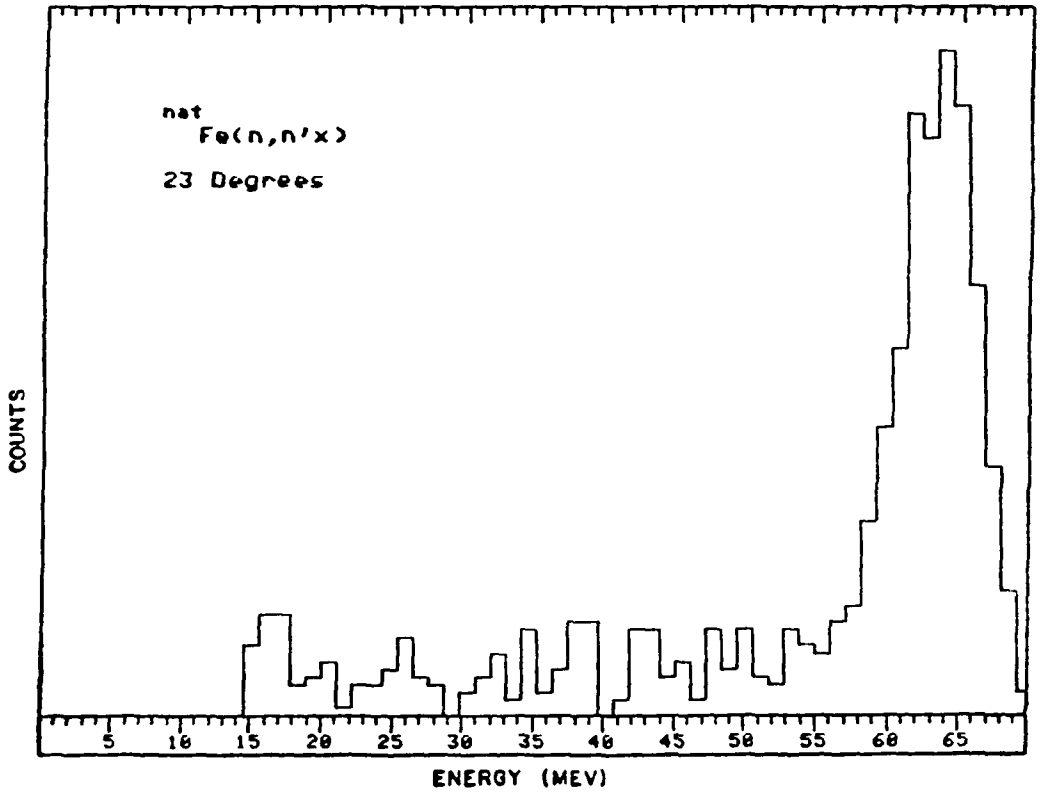

Figure 17

Fully analyzed (n,n'x) spectra from 22 to 24 degrees.

TABLE 2

FULLY ANALYZED SPECTRA DATA FROM 15° (LAB) TO 23° (2° BINS)

ENERGY (MeV)	EXCITATION ENERGY (MeV)	σ(15°) mb/sr-2MeV	Error mb/sr-2MeV	σ(17°) mb/sr-2MeV	Error mb/sr-2MeV
15.31	50.19	14.0	2.1	9.16	1.4
16.40	49.10	16.3	2.4	12.1	1.8
18.59	46.91	21.2	3.2	10.1	1.5
20.78	44.72	8.86	1.3	5.31	.79
22.90	42.60	19.9	3.0	7.23	1.1
25.15	40.35	17.7	2.7	8.68	1.3
27.34	38.16	20.2	3.0	7.72	1.2
29.53	35.97	16.0	2.4	7.72	1.2
31.71	33.79	21.4	3.2	11.6	1.7
33.90	31.60	14.7	2.2	10.6	1.6
36.09	24.41	24.8	3.7	13.0	2.0
38.28	27.22	30.8	4.6	6.27	.94
40.46	25.04	29.8	4.5	15.4	2.3
42.65	22.85	22.9	3.4	13.9	2.1
44.84	20.66	26.3	3.9	13.5	2.0
47.03	18.47	26.3	3.9	4.82	.72
49.21	16.29	34.9	5.2	26.1	3.9
51.40	14.10	30.2	4.5	27.0	4.1
53.59	11.91	32.0	4.0	22.7	3.4
55.78	09.72	18.4	2.8	16.9	2.5
57.96	07.54	22.9	3.4	24.1	3.6

TABLE 2 (Continued)

FULLY ANALYZED SPECTRA DATA FROM 15° (LAB) TO 23° (2° BINS)

ENERGY (MeV)	EXCITATION ENERGY (MeV)	σ(19°) mb/sr-2MeV	Error mb/sr-2MeV	σ(21°) mb/sr-2MeV	Error mb/sr-2MeV
15.31	50.19	4.65	.69	6.66	1.1
16.40	49.10	9.82	1.5	4.56	.74
18.59	46.91	6.72	1.1	2.26	1.2
20.78	44.72	3.62	.54	3.63	.58
22.90	42.60	5.17	.77	5.70	.91
25.15	40.35	9.82	1.5	10.3	1.6
27.34	38.16	7.75	1.2	6.74	1.1
29.53	35.97	6.20	.93	7.78	1.2
31.71	33.79	3.10	.47	7.78	1.2
33.90	31.60	7.24	1.1	5.18	.82
36.09	24.41	7.24	1.1	9.84	1.6
38.28	27.22	9.31	1.4	5.70	.91
40.46	25.04	6.72	1.1	11.9	1.9
42.65	22.85	5.17	.78	8.30	1.3
44.84	20.66	10.9	1.6	6.74	1.1
47.03	18.47	12.9	1.9	4.66	.75
49.21	16.29	18.6	2.8	9.33	1.5
51.40	14.10	16.0	2.4	14.0	2.2
53.59	11.91	5.69	.85	7.78	1.2
55.78	09.72	15.0	2.3	8.82	1.4
57.96	07.54	17.5	2.6	9.85	1.6

TABLE 2 (Continued)

FULLY ANALYZED SPECTRA DATA FROM 15° (LAB) TO 23° (2° BINS)

ENERGY (MeV)	EXCITATION ENERGY (MeV)	σ(23°) mb/sr-2MeV	Error mb/sr-2MeV
15.31	50.19	5.35	.86
16.40	49.10	6.56	1.1
18.59	46.91	2.18	.35
20.78	44.72	1.94	.31
22.90	42.60	1.94	.23
25.15	40.35	3.89	.62
27.34	38.16	2.18	.35
29.53	35.97	0.72	.12
31.71	33.79	3.16	.51
33.90	31.60	3.16	.51
36.09	24.41	2.18	.35
38.28	27.22	5.83	.93
40.46	25.04	0.48	.10
42.65	22.85	5.35	.86
44.84	20.66	2.91	.47
47.03	18.47	3.16	.51
49.21	16.29	4.13	.66
51.40	14.10	2.18	.35
53.59	11.91	4.86	.78
55.78	09.72	4.86	.78
57.96	07.54	9.40	

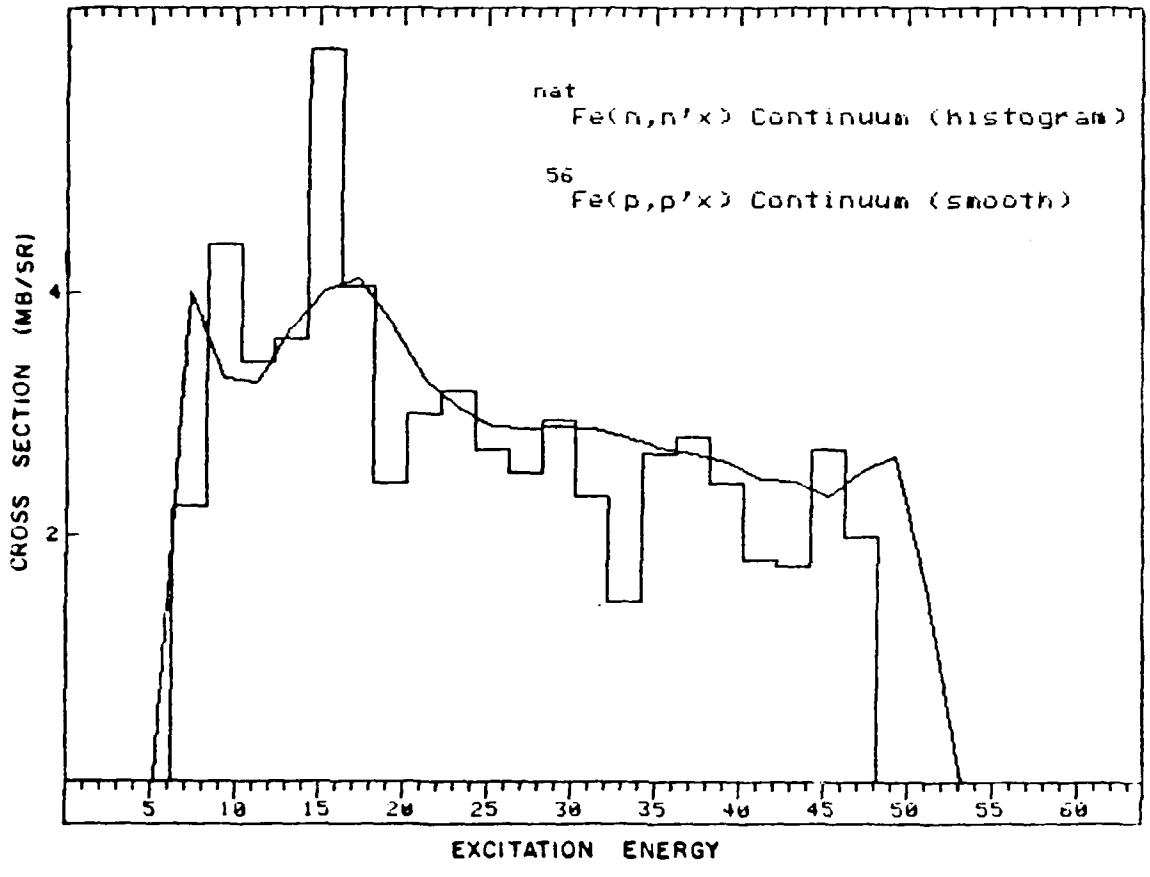

Figure 18

Comparison of $^{nat}Fe(n,n'x)$ results to $^{56}Fe(p,p'x)$ results at 20 degrees.

F.P. Brady and J.L. Romero, Progress Report to the National Science Foundation for Nuclear Physics Research, Grant PHY 7926282, July 1, 1979 to June 30, 1981.

F.P. Brady and J.L. Romero, Progress Report to the National Science Foundation for Nuclear Physics Research, Grant PHY 77-26050, July 1, 1977 to June 30, 1979.

F.P. Brady and J.L. Romero, Progress Report to the National Science Foundation for Nuclear Physics Research, Grant PHY 81-21003, Feb. 1, 1982-June 30, 1984.

V.R. Brown and V.A. Madsen, "Core Polarization in Inelastic Scattering and Effective Charges", Physical Review C, 11, 1976.

Thomas A. Cahill, Crocker Nuclear Laboratory Annual Report, 1981-82, UCD Department of Physics.

T.D. Ford, G.A. Needham, F.P. Brady, J.L. Romero, and C.M. Castaneda, "A Multiwire Chamber System for Measurements of Charged Particle Spectra," submitted for publication to Nuclear Instruments and Methods in Physics Research, Uppsalla, Sweden.

S.M. Grimes and R.C. Haight, "Charged-particle Emission in Reactions of 15-MeV Neutrons with Isotopes of Chromium, Iron, Nickel, and Copper," Physical Review C, 19, 1979.

J.A. Jungerman and F.P. Brady, "A Medium-Energy Neutron Facility," Nuclear Instruments and Methods, 89, 1970.

Alan D. Kirsch, "The Spin of the Proton," Scientific American, May 1979.

A.M. Lane, Nuclear Theory, New York: W.A. Benjamin, Inc., 1964.

Pierre Marmier and Eric Sheldon, Physics of Nuclei and Particles, New York: Academic Press, 1969.

David S. Saxon, Elementary Quantum Mechanics, San Francisco: Holden-Day, 1968.

G.R. Satchler, Introduction to Nuclear Reactions, New York: John Wiley and Sons, 1980.

G.R. Satchler, "New Giant Resonances in Nuclei," ORNL-TM-4347, Oak Ridge National Laboratory, Sept. 1973.

F. Sauli, "Principles of Operation of Multiwire Proportional and Drift Chambers," Lectures given in the Academic Training Program of CERN, Geneva, 1977.

J.L. Ullman et al., "Excitation of Isoscalar Giant Quadrupole Resonance in $^{118}Sn(\pi^+, \pi^-)$," Physical Review Letters, 51, 1983.

PART IX

BIBLIOGRAPHY

F.D. Becchetti, Jr., and G.W. Greenlees, "Nucleon-Nucleus Optical-Model Parameters, A>40, E<50 MeV," Physical Review, 182, 1969.

A.M. Bernstein, V.R. Brown and V.A. Madsen, "The Variation of Beta R with Probe Inelastic Hadron Scattering and the Adequacy of First-Order Calculations," Physics Letters, 106B, 1981.

A.M. Berstein, V.R. Brown and V.A. Madsen, "Neutron and Proton Transition Matrix Elements and Inelastic Hadron Scattering," Physics Letters, 103B, 1981.

F.E. Bertrand and R.W. Peelle, "Complete Hydrogen and Helium Particle Spectra from 30 to 60-MeV Proton Bombardment of Nuclei," Physical Review C, 8, 1973.

Fred E. Bertrand, "Excitation of Giant Multipole Resonances Through Inelastic Scattering," Annual Review of Nuclear Science, 26, 1976.

Fred E. Bertrand, "Giant Multipole Resonances-Perspectives After Ten Years," Nuclear Physics, A354 (1981).

F.E. Bertrand and R.W. Peelle, "Tabulated Cross Sections for Hydrogen and Helium Particles Produced by 62-MeV and 29 MeV Protons on ^{27}Al," ORNL-4455, 1969.

F.E. Bertrand and R.W. Peelle, "Tabulated Cross Sections for Hydrogen and Helium Particles Produced by 62-, 39-, and 29-MeV Protons on ^{54}Fe," ORNL-4469, Feb. 1970.

F.E. Bertrand and R.W. Peelle, "Tabulated Cross Sections for Hydrogen and Helium Particles Produced by 61-MeV Protons on ^{56}Fe," ORNL-4456, 1969.

Judith Binstock, "Parametrization of θ(tot), θ(0), and P(0) for 25-100 MeV np Elastic Scattering," Physical Review C, 10, 1974.

F.P. Brady, T.A. Ford, C.M. Castaneda, M.L. Johnson, G.A. Needham, and J.L. Romero, "A New Type of Neutron Detector Using Multiwire Chambers," Presented at the International Conference on Nuclear Data for Science and Technology, 6-10 Sept. 1982, Antwerp, Belgium.

F.P. Brady et. al., "A Multiwire Chamber System for Measurements of Neutron Spectra," Nuclear Instruments and Methods in Physics Research, 228, 1984.

[20] F.P. Brady et al., (1984) 91.

[21] J. Binstock, Physical Review C, 10 (1974).

[22] The equations [16] and [23] resulted from private communication between this author and F.P. Brady, 10/84.

[23] F.P. Brady et al., (1984) 92.

[24] F.E. Bertrand and R.W. Peelle, ORNL-4456, 1969, 1-37.

[25] F.E. Bertrand and R.W. Peelle, ORNL-4456, 1969, 36.

[26] G.R. Satchler, ORNL-TM-4347, (1973) 23, and F.E. Bertrand et al., Physics Letters, 80B, 3, (1979) 198-200.

[27] F.E. Bertrand et al., Physics Letters, 80B, 3, (1979) 198-200.

[28] Bertrand et al., (1979) 198-200.

[29] F.P. Brady et al., (1984) 91.

[30] F.P. Brady et al., (1984) 91.

[31] J. Rapaport, paper presented at the International Conference on Nuclear Data for Basic and Applied Science, Santa Fe, NM (May 13-17, 1985).

PART VIII

REFERENCES

[1] F.E. Bertrand, Annual Review of Nuclear Science, 26 (1976) 459.

[2] Bertrand, (1976) 461.

[3] F.E. Bertrand, Nuclear Physics, A354 (1981) 131c.

[4] Bertrand, (1976) 497-502.

[5] A.M. Lane, Nuclear Theory. New York: Benjamin, 1964, 79.

[6] Lane, (1964) 80.

[7] Lane, (1964) 80.

[8] Bertrand, (1976) 462.

[9] V.R. Brown, private communication with Dr. F.P. Brady, 4/85.

[10] A.B. Bernstein, V.R. Brown and V.A. Madsen, Physics Letters, 103B (1981) 256.

[11] F.P. Brady, private communication, 4/85.

[12] F.P. Brady et al., Nuclear Instruments and Methods in Physics Research, 228 (1984) 89-92.

[13] F.P. Brady et al., (1984) 89-92.

[14] V.R. Brown, private communication with F.P. Brady, 7/84.

[15] J.A. Jungerman and F.P. Brady, Nuclear Instruments and Methods, 89 (1970), 171.

[16] J.A. Jungerman, (1970), 171.

[17] T.D. Ford et al., submitted for publication to Nuclear Instruments and Methods in Physics Research, Uppsalla, Sweden.

[18] T.D. Ford et al.

[19] F.P. Brady et al., (1984) 89-92.

PART VII

CONCLUSION

At the conference for "Nuclear Data for Basic and Applied Science" in Santa Fe, NM (13-17 May 1985) Jacob Rapaport stated during his presentation:[31]

> "Among the nuclear studies that deserve attention, the following should be given high priority...The excitation of other giant resonances and their decomposition in terms of neutron and proton matrix elements is a topic that has not yet been studied thoroughly...it is something very much worthwhile to consider. To my knowledge there is no neutron inelastic scattering data for the excitation of giant resonances."

This study has provided the first preliminary data in this area. It has clearly demonstrated the feasibility of the (n,n'x) facility to measure the (n,n'x) spectra and compare neutron to proton matrix elements. With the improvements already discussed in Part VI, the resulting increase in statistics and energy resolution, will allow a more accurate and precise measurement of suspected giant resonances. Since the (n,n'x) facility is the only known operational setup in the world that measures (n,n'x), it is essential that the Neutron Group exploit the expertise already gained to continue experimentation with Fe and other nuclei of interest.

This change will result in a small increase in the overall energy resolution, but considering the other uncertainty factors involved, the possible gain in statistics far outweigh the resolution costs.

Increase Data Acquisition Time.

Even with the improvements mentioned above, increased time must be allowed for data acquisition with all types of targets and converters. In particular nearly equal time must be allowed for (a) and (b) below:

a. Fe target with CH_2 converter,

b. Fe target with carbon converter,

c. target empty with CH_2 converter, and

d. target empty with carbon converter.

A run of 60 to 72 hours should easily meet the above goals (44 hours of beam time was needed for this experiment).

Check for Multiple Scattering in the Fe Target

A short run should be made prior to the actual experiment to check for the effects of multiple scattering. Several thicknesses of iron should be used varying from 0.25 to 3 cm. After full analysis and comparison, the thickest target, with acceptable multiple scattering, should be for the full run. Using this procedure will provide a numerical factor for multiple scattering during later analysis and, should a thicker target be used, will provide better statistics with a relatively small increase in energy resolution.

improved cuts will allow fewer C(n,p) converter events to be included again simplifying the carbon subtraction process. This improved E-TOF array will also insure a better elimination of reactions caused by the neutron beam tail enhancing the entire energy spectra.

Statistics vs. Energy Resolution

In an experiment of this type, there is a constant struggle to improve statistics and yet keep the energy resolution small. Better energy resolution and/or statistics can be obtained by:

a. Increasing the thickness of the lithium production target from 66 mil to 119 mil. This will increase the resolution from .5 MeV to .65 MeV but increase the neutron count rate by almost a factor of two.

b. Decreasing the angle of acceptance for the (n,p) reaction at the converter. Since this is the single largest factor in improving the energy resolution, decreasing the angles upper limit from 15 to 7 degrees will reduce the energy resolution from 5 to 3 MeV. The corresponding decrease in statistics would be more than made up for by the factors above.

c. Increase the thickness of the CH_2 Converter. The amount of carbon in the CH_2 converter should be increased to the amount found in the carbon converter (per square cm.). Making this change will assist analysis in two ways. First, the number of protons produced will increase, thereby increasing statistics; second, the problems associated with the subtraction of carbon events at the converter will decrease since smoothing will not be required. This change will also simplify the energy loss equations for a proton going through the system since the energy losses for a CH_2 or C converter will be nearly equal.

PART VI

CHANGES TO PROCEDURE AND EQUIPMENT FOR IMPROVED (n,n'x) MEASUREMENT

Due to the experiences of conducting this experiment for the first time, the following recommendations are made to improve (n,n'x) results.

Measuring Mid-Angles Only

By specifically setting up the equipment as seen in figure 6 to look at laboratory angles of 15 to 40 degrees several of the problems encountered in the experiment could be resolved.

First, by conducting the experiment at the mid-angle range, many of the problems of the carbon (n,p') subtraction could be avoided. This is best seen in the energy vs count spectra where the effects of carbon (n,p) in the CH_2 converter fall off faster with increasing angle than those for the hydrogen (n,p) reaction. (This is because the C(n,px) are proportional to the elastic cross section.) At the higher angles, there is a decrease in the chance for error since it would require subtracting less carbon.

Second, these larger angles will not require the beam to pass through the MWC's. This would result in a decrease in overall background to be subtracted since beam (n,p') reactions at the MWC's windows would be avoided.

Finally, the set-up after the converter can be moved farther away from the Fe target. This will cut down on the number of angles that can be evaluated at one time and the solid angle at each angle, but will increase our ability to make more precise software cuts by widening group separations on the E-TOF arrays as seen in figure 11. These

The last uncertainty that can be calculated is due to the energy of resolution the E detectors (E1 and E2) to give the proper response when it stops an incident particle. Several mapping tests before the experiment demonstrated that the NE102 and NaI detectors had an energy resolution of 1.7 MeV for protons of approximately 50-55 MeV energy (50-55 MeV is the energy calculated for the proton as it strikes the detectors after passing through the system (see "Loss of Energy by Recoil Protons" above).

Together, the above independent energy uncertainties result in an overall predicted energy resolution of approximately 3 MeV.

Measured Energy Uncertainty

After completing the analysis of all data, the energy uncertainty, as measured at the elastic peak (FWHM), was 5 MeV. Since our prediction was 3 MeV, the discrepancy was attributed to more than expected (n,p) conversion error. To demonstrate this, runs were analyzed with an acceptance angle of 0 to 5 degrees. As expected, the uncertainty (FWHM) decreased to a value of 3.3 MeV with a corresponding decrease in statistics. Decreasing the angle of acceptance to 1 degree, or less, would clearly bring us very close to the value of calculated uncertainty due to factors other than conversion. However, for this experiment, decreasing the allowed conversion angle was not feasible, since the resultant decrease in count rate made analysis all but impossible except for the small angle bins.

with the calculation of [27] results in an energy uncertainty of approximately .6 MeV.

An uncertainty results from the varied energy loss of the recoil proton as it exits the converter after (n,p) conversion. This again is determined by the thickness of the converter and is calculated by use of the nonrelativistic stopping power equation (equation [27]). This uncertainty varies with energy and is approximately .85 MeV (at 50 MeV) for the CH_2 converter being used.

Another uncertainty results form the fact that the recoil neutrons from the Fe target do not come from an infinitely small point, but rather, from a 1.8 × 1.8 cm square. This produces an uncertainty as to where the (n,n'x) conversion actually took place in the target and therefore a possible variation in the incident angle of the n' as it struck the CH_2 converter from the target. The uncertainty in angle measured by the MWC's for the proton after the (n,p) reaction must also be included with these calculations along with the energy uncertainty due to the largest (n,p) conversion angle allowed. Using nonrelativistic kinematics, the energy uncertainty for these factors can be calculated by the equation[27]

$$E_p = E_n \cos 2\theta \qquad [28]$$

$$dE_n = -2\, E_p (\cos\theta)^{-3}\, d(\cos\theta)$$

$$\text{or} \quad dE_n/E_n = 2 \tan\theta d\theta$$

where $d\theta$ = the max angular error, and

θ = angle of maximum (n,p) conversion.

The possible angle errors described, after calculation, results in a total energy uncertainty factor of 2.14 MeV.

uncertainties in the system which effect the overall energy resolution possible. These uncertainties should be understood, theoretically predicted and allowed for in discussing results and making conclusions.

The first uncertainty to be allowed for is the minor variation in the energy of the H^+ beam coming from the cyclotron. In the past this ΔE was measured to attain a maximum value of .5 MeV.

The second uncertainty to be predicted is the spreading of the primary energy peak of the neutron beam coming from the Li production target. This peak spread is caused by the varied energy loss of the protons as they pass through the Li before collision and conversion. The magnitude of spreading of the $Li(p,n)^7Be$ peak is due mostly to the thickness of the production target (the thicker the target the more the possible energy loss) and is evaluated by use of the nonrelativistic stopping power equation.

$$-dE/dx = .1536\frac{(z^2)Z}{A\varepsilon}(\ell n\ 4\varepsilon)\ \frac{m_e c^2}{\langle I_{ADJ}\rangle}) - (\frac{c}{Z}) \qquad [27]$$

where z = charge of incident particle,

Z = charge of target nuclei,

A = atomic weight of target,

ε = Energy of incident particle/mass energy of incident particle,

$\langle I_{ADJ}\rangle = kZ = 14.33$ (charge of target nuclei) and

dx = density of target (.5 thickness of target).

For the lithium production target this results in an energy uncertainty of .33 MeV. There is also a tendency of the .43 MeV state in ^7Be to overlap and therefore spread the primary energy peak we wish to optimize. This effect has been measured in the past[29] and when combined

At 20 degrees the GR is centered at 15.7 MeV and therefore $\beta_L^2(100\%)$ is equal to .049. By using the Neutron Group's program "GNFIT", and subtracting an approximate continuum background, the total counts under the suspected GR was 81. Using the elastic peak cross section value from figure 14, 81 counts equates to a cross section value of 10.8 mb/sr. Running "DWUCK" with the proper parameters for the evaluation of a quadrupole resonance results in a value of σ(DWUCK) = 209.6 mb/sr. Putting this all together results in

EWSR% = .96.

This value seems high at first glance however, with our resolution it must be remembered that the σ(expt) includes a contribution from the other giant multipole resonances. Based on (p,p'x) analysis these resonances at an angle of 20 degrees are expected to make up approximately one third of the experimental GR hump.[27] After calculation

EWSR% (GQR) $\cong$ .63.

This value for the EWSR% is considered reasonable since measured values for (p,p'x) have resulted in EWSR% (GQR) of 50±10 (^{58}Ni), 40±10 (^{40}Ca) and 60±15 (^{10}Zr).[28] Since the EWSR% value is greater than 10%, and its magnitude is of reasonable value, indications are by EWSR% standards, the hump we are seeing is a GR and probably results mostly from GQR contributions.

Known Energy Uncertainties Contributing to Overall Energy Resolution

Calculation of the energy of the scattered neutron and resultant scattered proton, as they travel through the system, is one of the most important goals of the experiment. However, there are minor

section. As with the elastic peak data, this expected similarity result tends to validate the experimental and analysis method.

With the energy integrated cross section calculated, the experimental ratio of neutron to proton matrix elements can be calculated using equation [15]. This results in a value of M_n/M_p of.98 ± .16.

As can be seen in figure 18, the proton results exhibit a clear GR hump at 16.5 MeV, which includes both quadrupole, dipole and monopole contributions,[26] while for the (n,n'x) results, there is a possible GR structure near 15 MeV. Although, due to limited statistics, the presence of the GR is not conclusive, the sum rule calculations (equations [8] and [13]) will be made to better classify the structure we do see.

From equation [8] we know C must be greater than or equal to 10 in order for a collective excitation to be possible. Since the suspected GR for this experiment is located between 14.5 and 16 MeV then

$$C \cong 185/15 = 12.3.$$

Since C is greater than 10, by the sum rule it is possible that the observed hump in figures 15, 16, and 18 is a GR of mixed multipole nature.

In order to more precisely check the fraction of the EWSR strength exhausted we must use equation [13]

$$EWSR\% = \beta_L^2(expt)/\beta_L^2(100\%)$$

with

$$\beta_L^2(expt) = \sigma(expt)/\sigma(DWUCK)$$

and

$$\beta_L^2(100\%) = .74\ MeV/E \text{ from equation [12].}$$

TABLE 3

CONTINUUM CROSS SECTIONS AT 20° (LAB)

ENERGY (MeV)	EXCITATION ENERGY (MeV)	σ(20°) mb/sr-2MeV	Error mb/sr-2MeV
15.31	50.19	4.58	.73
16.40	49.10	5.99	.96
18.59	46.91	5.67	.91
20.78	44.72	3.05	.49
22.90	42.60	4.47	.72
25.15	40.35	7.96	1.3
27.34	38.16	5.88	.94
29.53	35.97	5.45	.87
31.71	33.79	3.16	.51
33.90	31.60	5.01	.80
36.09	24.41	5.78	.92
38.28	27.22	6.10	.98
40.46	25.04	7.41	1.2
42.65	22.85	5.34	.05
44.84	20.66	7.08	1.1
47.03	18.47	7.19	1.2
49.21	16.29	11.66	1.9
51.40	14.10	11.99	1.9
53.59	11.91	5.34	.85
55.78	09.72	9.70	1.6
57.96	07.54	11.12	1.8

B.A. Watson, "Optical-Model Analysis of Nucleon Scattering from 1p-Shell Nuclei between 10 and 50 MeV," Physical Review, 182, 1969.

C.I. Zanelli, P.P. Urone, J.L. Romero, F.P. Brady, M.L. Johnson, G.A. Needham, and J.L. Ullmann, "Total Non-elastic Cross Sections of Neutrons on C, O, Ca, and Fe at 40.3 and 50.4 MeV," Physical Review C, 23, 1981.

APPENDIX I

Paper Presented at the International Conference on

Nuclear Data for Basis and Applied Science,

Santa Fe, NM (May 13-17, 1985)

^{nat}Fe(n,n'x) SPECTRA AT 65.5 MeV

M.A. HAMILTON, T.D. FORD, F.P. BRADY, J.L. ROMERO,
C.M. CASTANEDA AND J.L. DRUMMOND
Department of Physics and Crocker Nuclear Laboratory
University of California, Davis, CA 95616

Abstract The first spectra from the U.C. Davis (n,n'x) detection facility are presented for 65.5 MeV incident neutrons on a ^{nat}Fe target. Analysis has been conducted from 14 to 24 degrees and cross section comparisons are made between (n,n'x) and (p,p'x) data at 61 MeV. Evidence of a (n,n'x) Giant Resonance (GR) has been found and the ratio of neutron to proton matrix elements has been obtained.

INTRODUCTION

The excitation of Giant Resonances and continuum spectra by various particles have been of particular interest in recent years. The unique combination of a nearly monoenergetic neutron beam and the Multiwire Chamber Neutron Detection (MWC) Facility[1] at Crocker Nuclear Laboratory has made it possible, for the first time, to measure the (n,n'x) continuum and extract resonance cross sections. It is generally believed that (n,n'x) cross sections for a given angle will compare in shape and magnitude with (p,p'x) data. That conclusion is supported by the results presented here.

EXPERIMENT

The experiment was conducted at the Crocker Nuclear Laboratory 76 inch isochronous cyclotron using the ^{7}Li(n,p)^{7}Be neutron beam facility. The collimated neutron beam, after passing through the target, continues on to a beam intensity monitor. Neutrons scattered between 8 and 42 degrees are intercepted by the (n,n'x) facility (figure 1). A 6mm lead sheet and Veto MWC set in anti-coincidence with the rest of the system ensure that (n,p) reactions at the target are excluded.

A percentage of the neutrons striking the CH_2 converter undergo a (n,p) reaction and the resultant proton is tracked by MWC1, the ΔE detector and MWC2 before striking the E detector.

Data is collected, event by event, into CAMAC interfaced to a PDP 15/40 computer and stored on 7 track tape. During the experiment ^{nat}Fe, CH_2, C, and empty target runs were conducted. Runs were also made using a thin carbon converter with the ^{nat}Fe target and no target. Approximately 44 hours of data were acquired.

ANALYSIS

Initial software cuts on the raw data events in the ΔE and TOF-E matrices were made to eliminate non-peak neutron beam events and other than proton events.

Event by event, the two x-y coordinates supplied by the MWCs, allow the trajectory of the protons from the converter to be calculated along with the angle of the n' from the target. Using the energy value from the E detector and this angle the energy of the n' is calculated.

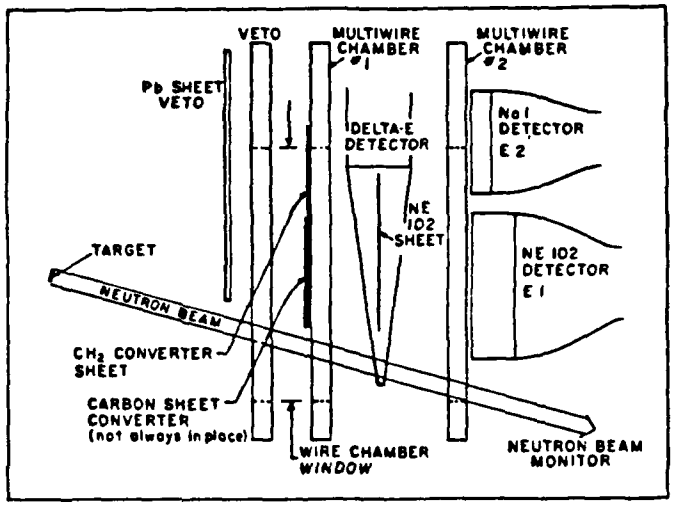

Fig. 1. Top view of apparatus

Binstock's parameterization[2] of the n-p differential cross sections is used to calculate the energy dependence of the conversion efficiency. Analyzed data were stored by 2 degree bins with final analysis having been completed between the angles of 14 and 24 degrees. It was found that even with the long run time, insufficient C converter data were taken. For the forward angles, C elastic neutron events (from the CH_2) had a large effect making up approximately 20% of the continuum. For statistical reasons we had to smoothe the C data over a range of angles before subtracting.

RESULTS

Spectra produced were similar in nature to that found in figure 2. The large FWHM on the elastic peak is caused by the large allowed angle of acceptance for the (n,p) at the converter. A smaller angle of acceptance would improve the energy resolution but with a corresponding decrease in statistics.

Normalization of the elastic peak cross sections was accomplished by use of a combination of Bechetti and Greenless optical

^{nat}Fe(n,n'x) SPECTRA AT 65.5 MeV

model (OM) equations as found in DWUCK and experimental (p,p) results of Bertrand and Peelle[3] at 61 MeV. First, the (n,n) results at 15 degrees were normalized to the OM cross section prediction for that angle. Using this 15 degree value, all other elastic peak cross sections were calculated. As seen in Fig. 3, the (n,n) results compare nicely to the OM shape. The (p,p) OM and experimental elastic results are also shown. The mean ratio of the (p,p) OM prediction to the measured (p,p) elastic data (averaged over the angles of 15 to 24 degrees) was calculated to obtain a factor to renormalize the (n,n) OM predictions. Finally the (n,n) datum were normalized to the 15 degree renormalized neutron OM prediction as shown in Fig. 4.

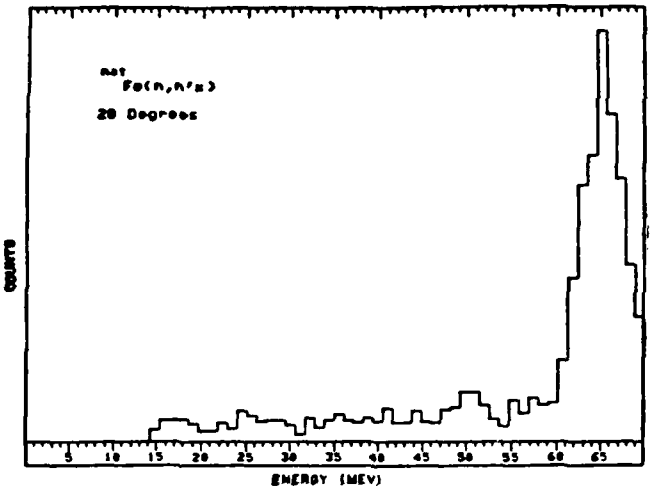

Fig. 2. Fe(n,n'x) at 20° and 65.5 MeV

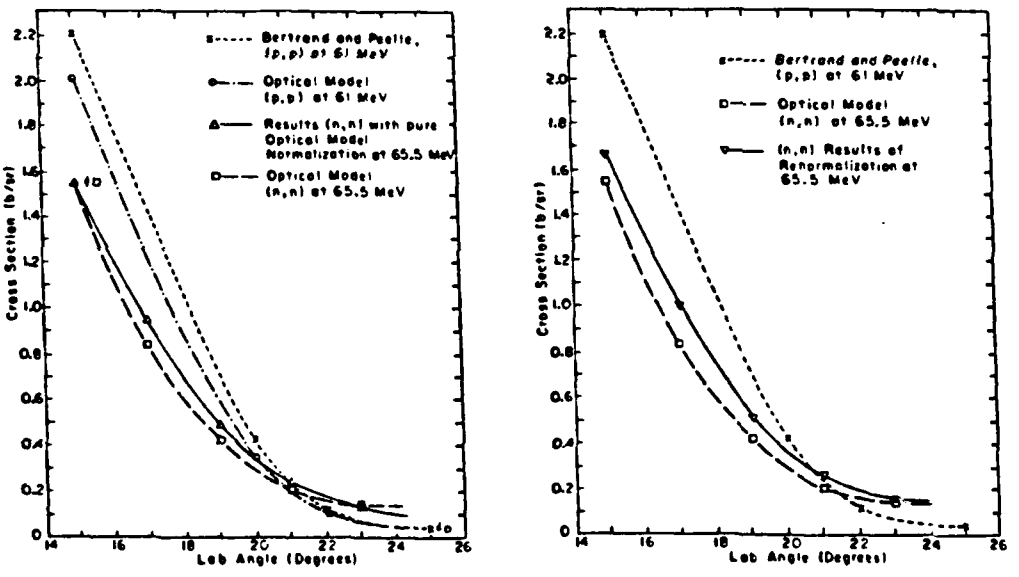

Fig. 3 and 4. OM compared to elastic (p,p) and (n,n) results

A comparison of the (n,n'x) and (p,p'x) continuum spectra, both at 20 degrees, is shown in Fig. 5. The shape and cross sections are very similar in appearance and magnitude. The proton results exhibit a clear GR hump at 16.5 MeV, while for the (n,n'x) results, there is a possible GR near 15 MeV. Statistical uncertainties in the continuum range from 10% to 15%. There are additional systematic uncertainties due to the carbon subtraction (~2-9%) and in the absolute normalization (~7%).

The energy integrated 20 degrees (p,p'x) cross section has a value of 138.2 mb/sr (±1.5 mb/sr) and (n,n'x) results in a value of 139.6 mb/sr (±18 mb/sr). For a nuclei such as ^{nat}Fe it is expected that the ratio of the neutron to proton multipole matrix elements should be close to N/Z or 1.15.[4] Using the above data, assuming $V_{np} = 3\ V_{pp}$, and using the formula

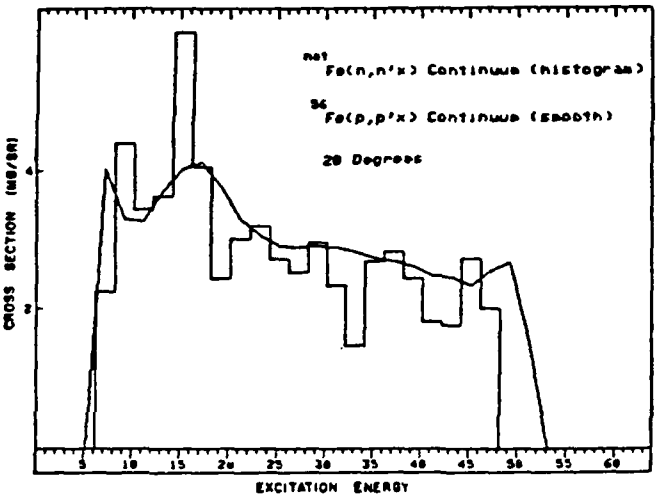

Fig. 5. Fe(p,p'x) - (n,n'x) comparison

$$\frac{\sigma(n,n'x)}{\sigma(p,p'x)} \equiv \frac{V_{np}M_p + V_{pp}M_n}{V_{pn}M_n + V_{pp}M_p}$$

results in an experimental value of $M_n/M_p = .98 \pm .16$.

In conclusion, the results presented demonstrate the feasibility of the (n,n'x) facility at Crocker Nuclear Laboratory. Improvements are already planned that will increase statistics along with improving energy and angular resolution.

The support of the NSF Grant PHY 81-21003 is greatly appreciated.

REFERENCES

1. F.P. Brady et al., NIM 228, p. 89-93 (1984).
2. J. Binstock, Phys. Rev. C10, 1, p. 19 (1974).
3. F.E. Bertrand and R.W. Peelle, ORNL-4456 (1969).
4. A.M. Berstein et al., Phys. Lett. 103B, 255-258 (1981).

END

FILMED

8-85

DTIC